

On the occurrence of amphibolite-facies sapphirine, spinel, phlogopite, anorthite, and corundum in the Wet Mountains, Colorado, USA

Richard M. Palin^{a,*}, Zachary Palmer^b, Christopher Holm-Denoma^c, David Hernández-Uribe^d, Juan David Hernández-Montenegro^{e,f}

^a Department of Earth Sciences, South Parks Road, Oxford OX1 3AN, United Kingdom

^b Department of Geology and Geological Engineering, Colorado School of Mines, Golden, CO 80401, USA

^c United States Geological Survey, Denver Federal Center, Denver, CO 80225, USA

^d Department of Earth and Environmental Sciences, University of Illinois, Chicago, IL 60607, USA

^e Departamento de Geociencias, Universidad Nacional de Colombia, Bogotá, Colombia

^f Division of Geological and Planetary Sciences, California Institute of Technology, Pasadena, CA 91125, USA

ARTICLE INFO

Keywords:

Sapphirine

Spinel

Contact metamorphism

Granite

Pseudosection

ABSTRACT

The Wet Mountains, southern Colorado, expose Mesoproterozoic metamorphic and magmatic rocks that record the early deformational history of the west-central continental USA and growth of Laurentia. Of particular petrological interest are halogen-enriched metamorphic rocks adjacent to the San Isabel A-type granite, situated in the southern Wet Mountains, which contain sapphirine, spinel, phlogopite, anorthite, and corundum. Conventional thermobarometry and phase diagram-based thermodynamic modeling indicates peak pressure–temperature (P – T) conditions of metamorphism within the upper amphibolite facies (~ 750 – 770 °C) at middle-crustal pressures (~ 6 – 7 kbar), and in-situ U–Pb geochronology of monazite constrains peak metamorphism to c. 1340–1320 Ma. These sapphirine-hornfels units are younger than metamorphic lithologies elsewhere in the southern Wet Mountains (c. 1430 Ma), but only slightly post-date the timing of intrusion of the granite itself (1362 ± 7 Ma). These rocks are thus interpreted to be of contact metamorphic origin, with high F contents in mica and amphibole interpreted to record metasomatism in the middle crust by halogen-rich fluids expelled by the San Isabel granite. However, as the temperature of emplacement and crystallization of the granite likely did not greatly exceed 800–850 °C, these rocks document an unusual occurrence of normally granulite-facies and (ultra)high-temperature metamorphic minerals stabilizing at lower grade. Thus, caution must be used when using such parageneses as field indicators of geodynamic settings associated with extreme heat flow, such as continental rifting and/or voluminous emplacement of dry, mafic magma.

1. Introduction

The metamorphic facies concept (Eskola, 1914) is a cornerstone of modern petrology and allows straightforward identification of metamorphic rocks in the field, interpretation of the tectonic processes that formed them, and thus insight into the geodynamic history of a terrane. This facies system categorizes rocks in terms of the absolute pressure–temperature (P – T) conditions reached during metamorphism, allowing determination of the geothermal gradient along which peak conditions lie (Weller et al., 2013). Indeed, many geological environments are characterized by specific geothermal gradients (dT/dP): for example, metamorphism of subducted oceanic crust typically occurs at

cold geothermal gradients of ~ 15 °C/kbar and ~ 35 °C/kbar, depending on factors such as slab age, slab dip angle, and convergence rate; metamorphism of crustal materials during continental collision is typically characterized by moderate values of ~ 35 – 75 °C/kbar; and metamorphism along high or ultrahigh geothermal gradients, where elevated temperatures are reached at relatively low lithostatic pressures (> 75 °C/kbar), typically characterizes contact metamorphism. In the latter case, a source of heat, such as magma, is typically brought directly against a relatively cool rock at medium to shallow crustal levels.

The interpretation that metamorphic rocks can reach (and sustain) absolute temperatures exceeding ~ 900 °C at relatively shallow depths within the continental crust is a recent development in the petrological

* Corresponding author.

E-mail address: richard.palin@earth.ox.ac.uk (R.M. Palin).

<https://doi.org/10.1016/j.lithos.2023.107024>

Received 13 September 2022; Received in revised form 30 December 2022; Accepted 10 January 2023

Available online 20 January 2023

0024-4937/© 2023 The Authors. Published by Elsevier B.V. This is an open access article under the CC BY license (<http://creativecommons.org/licenses/by/4.0/>).

community (Harley, 1998), although is now unequivocal based on mineral assemblages with stability ranges that have been constrained experimentally. Such metamorphic rocks are described as ultra-high temperature (UHT) and represent critical petrological evidence for extreme thermal events within the geological record (e.g. Kelsey and Hand, 2015). Certain metamorphic minerals are often found in UHT metamorphic rocks and have become known by researchers as potentially diagnostic indicators of these conditions, including sapphirine [(Mg,Al)₈(Al,Si)₆O₂₀] (Harley, 1998). Other metamorphic minerals, such as spinel, osumilite, corundum, and Al-rich orthopyroxene can occur in sub-900 °C rocks, but still record high-temperature metamorphism typically characteristic of the granulite facies (Waters, 1988).

Previous studies of Cu- and Zn-rich metasedimentary rocks from the southern Wet Mountains, south-central Colorado, have reported sapphirine-, corundum-, spinel-, and orthopyroxene-bearing assemblages that occur in close proximity to the Mesoproterozoic (c. 1360 Ma) San Isabel A-type granite intrusion (Taylor et al., 1984), although the *P-T* conditions of their formation are unknown. Whether or not these assemblages formed before, during, or after magmatism is also uncertain, as no geochronology has been performed on the metamorphic aureole, although age data exist for other metamorphic units elsewhere in the Wet Mountains. Specifically, it is unclear whether the rocks in question formed due to contact metamorphism – perhaps driven by emplacement of the San Isabel granite – or whether their mineral assemblages formed before (or after) magma emplacement, thus representing regional metamorphic signatures of a hitherto unrecognized high-temperature tectonic event in the history of east-central Colorado.

Here, we combine the results of field investigation, petrology, conventional- and phase diagram-based thermobarometry, and U-Pb geochronology of monazite to provide new insight into the geological history of the San Isabel region of the southern Wet Mountains and the thermo-chemical conditions at which nominally high-temperature minerals can unexpectedly stabilize. Metasedimentary lithologies

containing sapphirine are focused upon, owing to its rarity in metamorphic rocks worldwide and its potential usefulness as an indicator of (U)HT thermal conditions in the crust (Kelsey and Hand, 2015), although a range of lithotypes have been examined. Despite much study in recent years, key questions about the ages and evolution of metamorphic and magmatic rocks in the Wet Mountains are unresolved (cf. Herna'ndez-Montenegro et al., 2019; Levine et al., 2013), which have implications for competing broad-scale lithospheric models of the geological evolution of the central U.S.A. since the Late Paleoproterozoic.

2. Geological background

The west-central U.S.A. and Colorado Front Range preserve many metamorphic, magmatic, and deformational events associated with formation of Laurentia, which at c. 2 Ga was comprised of several Archean terranes and Paleoproterozoic suture zones (Fig. 1a; Hoffman, 1988). At this time, the southernmost margin of Laurentia was represented by the Wyoming Craton – an ancient cratonic nucleus (c. 3.5–2.5 Ga; Frost et al., 1998) – against which four crustal terranes/microcontinents were accreted due to sequential ocean closure and collisional orogeny during the Mesoproterozoic (Whitmeyer and Karlstrom, 2007). From northwest to southeast, these comprise the Mojave, Yavapai, Mazatzal, and Grenville Provinces (Fig. 1a, b).

The northwesternmost Mojave Province is dominated by metasedimentary gneisses (Wooden and Miller, 1990) with Mesoproterozoic protolith depositional ages of c. 1.79–1.75 Ga (Wooden et al., 2013). However, whole-rock Nd model ages for some meta-igneous suites range from c. 2.7 to 1.7 Ga, with a mean age of c. 2.2 Ga (Coleman et al., 2002), indicating the presence of older (Archean) components within the terrane itself. The Mojave Province accreted to the southern edge of the Wyoming Craton at c. 1.8 Ga (Fig. 1a; Whitmeyer and Karlstrom, 2007).

The Yavapai Province represents a structurally complex

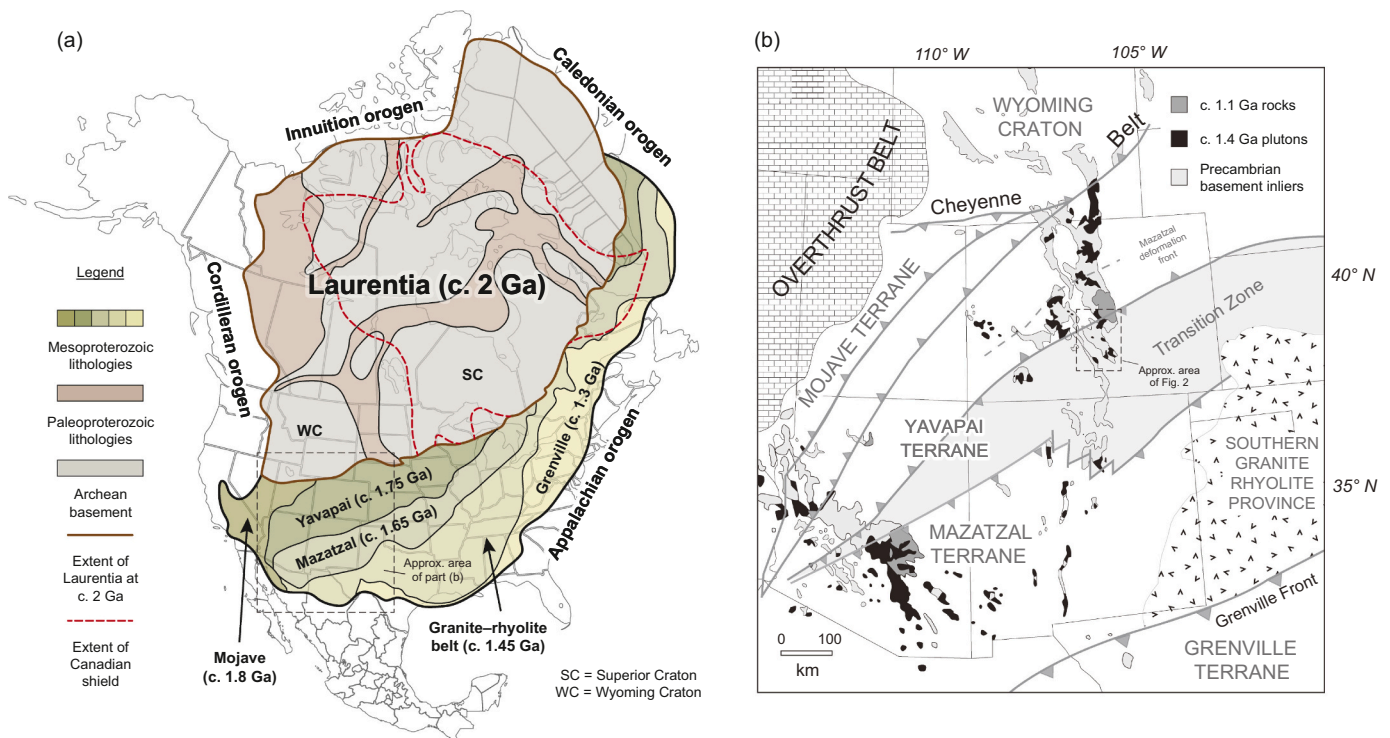


Fig. 1. Geotectonic setting of the Colorado Front Range. (a) Terrane map of the U.S.A., Canada, and Greenland, which is shown in its position prior to opening of the Atlantic Ocean. The extent of Laurentia at c. 2 Ga is shown by a bold brown line, and the Canadian Shield is outlined by a red dashed line. (b) Province map of the west-central U.S.A. modified from Daniel et al. (2013). (For interpretation of the references to colour in this figure legend, the reader is referred to the web version of this article.)

amalgamation of juvenile arc terranes with Nd model ages of c. 2.0–1.8 Ga (Bennett and DePaolo, 1987) that accreted to the southeastern edge of the Wyoming craton at c. 1.78 Ga (Jones et al., 2010), forming a prominent deformational zone passing through Colorado, Arizona, and New Mexico (Fig. 1b). This event is known as the Yavapai orogeny. Lithologies exposed within this collision zone in the Colorado Front Range preserve upper-amphibolite facies metamorphism indicative of formation in the middle crust (e.g. Mahan et al., 2013). The final stages of this accretional orogeny are documented by syn- to post-orogenic S-type granites emplaced throughout the belt at c. 1.70–1.65 Ga (Anderson and Cullers, 1999), likely following crustal thickening, heating, and partial melting of deeply buried metasedimentary lithologies.

The Mazatzal Province contains meta-igneous rocks with Nd model ages of c. 1.80–1.70 Ga (Bennett and DePaolo, 1987) and is thought to

have accreted to the southern edge of the Yavapai Province at c. 1.66–1.60 Ga, marking an event termed the Mazatzal orogeny (Amato et al., 2008). Deformational features directly related to this terrane-accretion event can be observed a significant distance within the Yavapai Province, and are demarcated by a southwest–northeast trending line termed the Mazatzal deformation front (Fig. 1b: Shaw and Karlstrom, 1999). More intense deformation, marking the position of the Yavapai–Mazatzal suture zone, occurs in southern Colorado.

The Grenville Province lies south of the Mazatzal Province and fused to the southern edge of Laurentia at c. 1.30 Ga, as constrained by termination of emplacement of subduction-related calc-alkaline magmas in the southern edge of the Mazatzal Province (Rivers, 2008). However, in the intervening period between termination of the Mazatzal orogeny and initiation of the Grenville orogeny, much of Colorado

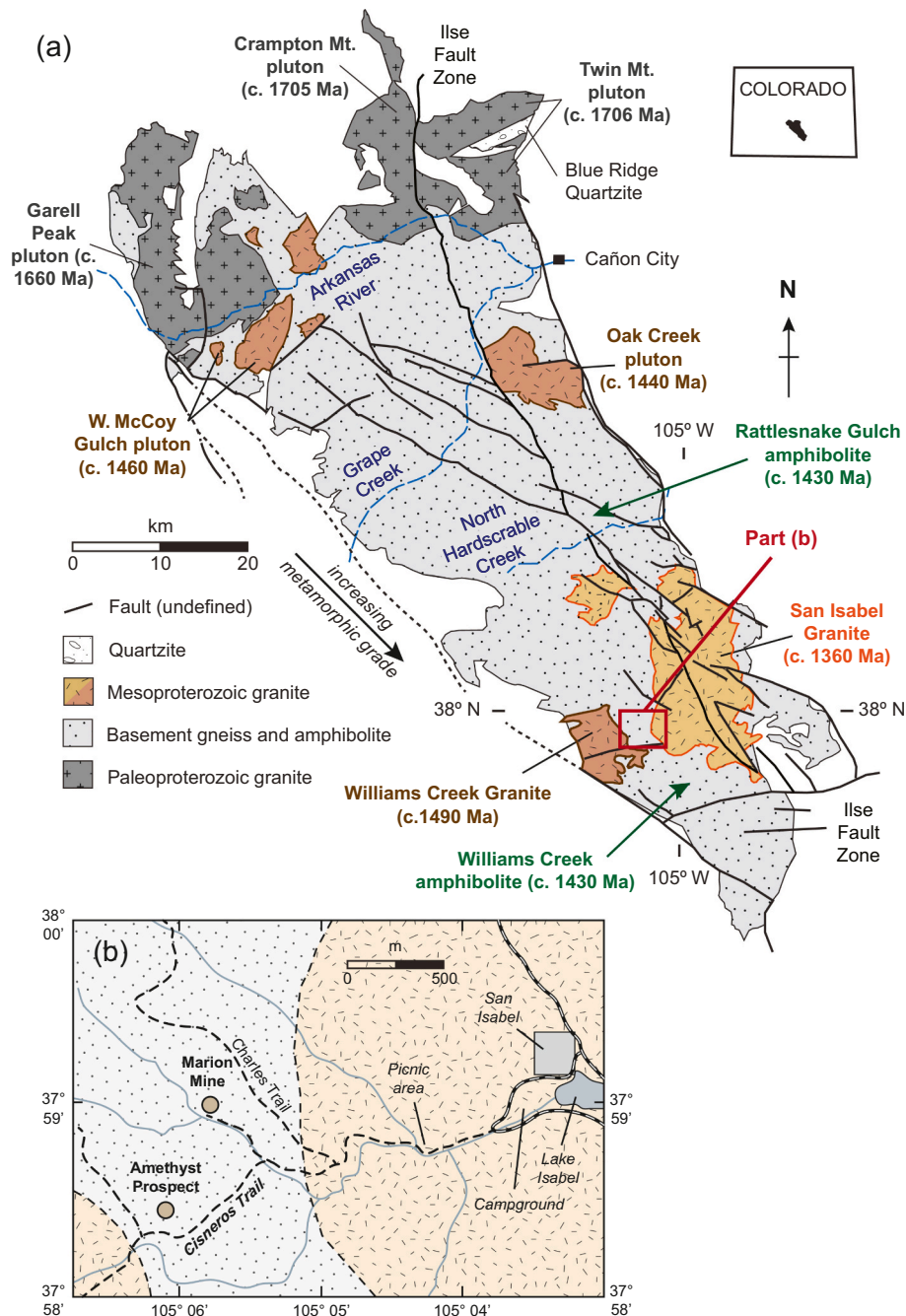


Fig. 2. Geological map of the Wet Mountains (a) Major lithostratigraphic units within the Wet Mountains (after Jones et al., 2010). (b) Location of the Marion Mine and Amethyst Prospect localities with respect to the approximate boundary of the San Isabel granite.

(including the Wet Mountains) records extensive metamorphism and magmatism at c. 1.50–1.35 Ga (e.g., Daniel et al., 2013; Jones et al., 2010), the cause of which is strongly debated. Exposures of voluminous c. 1.4 Ga granite plutons in the Rocky Mountains are commonly foliated (e.g., Aleinikoff et al., 1993) and spatially associated with ductile shear zones (Jessup et al., 2006; Selverstone et al., 2000; Shaw et al., 2001), suggesting a period of intense deformation and reactivation of older tectonic discontinuities. Recently documented metasedimentary rocks with north-vergent fold-and-thrust geometries that formed at c. 1.45 Ga in New Mexico (Aronoff et al., 2016) imply that there may be a hitherto poorly understood orogenic event that affected the south-central USA during the Mesoproterozoic, known as the Picuris orogeny, although debate remains as to the spatial extent and tectonic driving forces behind this event.

2.1. Geological history of the Wet Mountains

The Wet Mountains lie within the Yavapai Province, south of the Mazatzal deformation front (Fig. 1a), and contain a wide variety of metamorphic and magmatic rocks. Together, this terrane constitutes an exhumed and tilted section through the Mesoproterozoic continental crust, and exhibits increasing metamorphic grade from northwest to southeast (Fig. 2a; Siddoway et al., 2000; Jones et al., 2010). Aeromagnetic data reveal numerous southwest–northeast trending lineaments in the subsurface geology that have orientations consistent with structures developed throughout Colorado associated with the Yavapai and/or Mazatzal accretion events (Oshetski and Kucks, 2000), although limited previous geochronology in the region suggest that both metamorphism and magmatism have temporal affinity to the Picuris orogeny, as described below. Most of the metamorphic basement in the Wet Mountains is dominated by metasedimentary and metavolcanic gneisses, interpreted to be strongly deformed juvenile arc crust, alongside rarer calc-silicate gneisses and mafic gneisses/amphibolites (Jones et al., 2010). Strong positive gravity anomalies throughout the Wet Mountains also suggest the presence of voluminous plutonic rocks in the shallow subsurface (Pardo et al., 2008), indicating that magmatism may have been more widespread than the current level of surface exposure implies (Fig. 2a).

The northernmost section of the Wet Mountains exposes the only Paleoproterozoic plutons in the region, which are now weakly foliated and have gradational contacts with host felsic schist and gneiss (Siddoway et al., 2000). These comprise the c. 1.71 Ga Twin Mountain and Crampton Mountain granite plutons, and the c. 1.66 Ga Garell Peak granodiorite pluton (Fig. 2a; Bickford et al., 1989). Younger granitoids (the West McCoy Gulch pluton: c. 1.46 Ga) have sharper cross-cutting contacts with adjacent country rock and have poorly defined (if any) deformation features (Jones et al., 2010). Metamorphic units in this region are medium grade, with cordierite-, sillimanite-, and Mn-Fe-andalusite-bearing pelitic schists recording peak P – T conditions of ~3.5 kbar and ~600 °C (Siddoway et al., 2000).

The central section of the Wet Mountains, between the Arkansas River and North Hardscrabble Creek, mostly exposes middle-crustal quartzofeldspathic gneiss, with rarer outcrops of amphibolite in Rattlesnake Gulch (Fig. 2a). Geothermobarometry and U–Pb zircon geochronology performed on these metamafic units indicates peak metamorphism at ~5 kbar and ~650 °C, at c. 1.43 Ga (Jones III et al., 2015). Alongside the metamorphic host lithologies, the central section of the Wet Mountains exposes the Oak Creek and West McCoy Gulch two-mica monzogranite plutons, which were emplaced at c. 1.44 Ga (U–Pb zircon: Bickford et al., 1989). These plutons have gradational contacts with country rocks, indicating emplacement at middle-crustal levels below the brittle–ductile transition (Siddoway et al., 2000).

The southern section of the Wet Mountains, which represents the focus area of this study, is more lithologically diverse than the central and northern sections. Siddoway et al. (2000) described multiple suites of Mesoproterozoic granitoids in this region: one exposed as networks of

sills and dikes, and two others being plutons exposed in the far southeast (Fig. 2a). One of these, the San Isabel intrusion, is a largely undeformed hornblende–biotite monzogranite that crystallized at c. 1.36 Ga (U–Pb zircon: Bickford et al., 1989; Cullers et al., 1992). Geochemically, it has an A-type (anorogenic) affinity, with a weak Eu anomaly indicating derivation via partial melting of a mafic source rock (Cullers et al., 1992), and the depth of emplacement at the current level of exposure has been constrained by Al-in-hornblende barometry to be ~17–23 km (Cullers et al., 1992). It is younger than all other magmatic units in the Wet Mountains, including the Williams Creek Granite, which is located just to the southwest (Fig. 2a). The Williams Creek Granite is a coarse-grained porphyritic granite with a U–Pb zircon crystallization age of c. 1.49 Ga (Bickford et al., 1989), indicating that it has closer temporal affinity to the Oak Creek and West McCoy Gulch plutons in the central and northern sections of the Wet Mountains.

The metamorphic grade reached by basement gneisses in the southern section of the Wet Mountains is slightly higher than the central and northern sections. Evidence for partial melting and high-temperature metamorphism has been widely documented at the outcrop, hand sample, and thin section scale, with temperatures for peak metamorphism in pelitic migmatites around Williams Creek reported to be ~700–720 °C at ~5–6 kbar (Levine et al., 2013). By contrast, mineralized metamorphic country rocks immediately adjacent to the San Isabel Granite pluton were studied in moderate detail by USGS geologists in the mid- to late-1980s for their ore-bearing potential, but have since received little attention. A highly diverse suite of lithologies occurs in spoil heaps and in-situ exposures at the Amethyst Prospect and Marion Mine localities, both of which lie within 500 m of the inferred granite–country rock contacts (Fig. 2a), although the three-dimensional relationships between these blocks of metamorphic country rock and the intrusion itself remain uncertain. Poor exposure in the field area limits the potential for mapping of the morphology of this contact, such that it is unclear whether these blocks represent roof pendants, kilometer-scale xenoliths, or country rock protruding upwards through the pluton floor. Metasedimentary samples contain combinations of sapphirine, orthopyroxene, cordierite, spinel, and corundum, although no quantitative thermobarometry or geochronology has been performed on these samples. As such, neither the P – T conditions of equilibration nor the age of formation with respect to the geological history of the Wet Mountains are known.

3. Petrography and mineral chemistry

3.1. Field relations and outcrop localities

Forty samples of metamorphic rocks were collected during two field seasons in the Wet Mountains. Of these, six lithologies were focused on in detail to provide quantitative constraints on the P – T conditions and age and mechanism of metamorphism. Samples were collected from the Marion Mine and Amethyst Prospect localities, which are situated close to outcrops of the San Isabel granite and are presumed to lie within its contact metamorphic aureole (Fig. 2b).

Exposure is generally poor in the Wet Mountains due to extensive forestation, although the Marion Mine contains large sequences of bedrock in ~150-m-tall cliff sections along Amethyst Creek (Fig. 2b). Most lithologies collected from this locality were sampled in-situ from these cliff faces, although some come from spoil heaps situated at the base of this cliff. These spoil heaps are associated with the main underground workings; as such, the samples obtained from each are confidently assumed to have been removed from the adjacent country rock, and so represent the geology of the region.

Exposure of bedrock at the Amethyst Prospect is minimal, as the locality comprises an old mine opening, abandoned cabin, and associated spoil heap. Nonetheless, some metasediments occur as large (>1–10 m) blocks, presumably in-situ. Some lithologies were collected from the spoil heap, which akin to that at the Marion Mine is assumed to

contain rock types existing immediately beneath the surface, and thus within the metamorphic aureole of the intrusion.

3.2. Analytical procedures

Bulk-rock compositions were determined for samples 17SIMM01 (amphibolite), 17SIMM02 (garnet–biotite gneiss), 17SIMM04 (calc-silicate), 17SIAP02 (sapphirine hornfels), 17SIAP04 (marble), and 17SIAP09 (sapphirine hornfels) by combined X-ray fluorescence (XRF) (major elements) and inductively coupled plasma optical emission spectrometry (ICP-OES) (minor and trace elements) at Actlabs in Ontario, Canada. Major element oxide composition data are given in Table 1, and complete analyses including minor, trace, and rare earth element contents are given in Table S1. Mineral compositional data in each sample were obtained via electron probe microanalysis (EPMA) on a JEOL 8900 microprobe housed at the Microbeam Laboratory at the United States Geological Survey, Denver, Colorado, U.S.A. Representative mineral compositions for Marion Mine samples are given in Table 2, and those from Amethyst prospect samples are given in Table 3. Detail concerning both analytical procedures are given in the Supplementary Information.

Mineral abbreviations are as follows: An – anorthite; Bt – biotite; Cal – calcite; Ccp – chalcopryrite; Cpx – clinopyroxene; Chu – clinohumite; Crn – corundum; Dol – dolomite; Fo – forsterite; Grt – garnet; Ilm – ilmenite; Kfs – K-feldspar; Mt. – magnetite; Phl – phlogopite; Ple – pleonast; Pl – plagioclase; Prg – pargasite; Py – pyrite; Qtz – quartz; Rt – rutile; Sp – spinel; Spr – sapphirine; Ts – tschermakite.

3.3. Marion Mine

Lithologies observed in cliff faces and spoil heaps at the Marion Mine comprised metabasites (amphibolite), various metasedimentary rocks

(garnet–biotite gneiss, garnet–cordierite gneiss, and calc-silicates), and granitic orthogneiss. However, despite reports by previous workers (Raymond et al., 1980), no sapphirine-bearing metasediments were found.

3.3.1. 17SIMM01 – Amphibolite

Sample 17SIMM01 contains clin amphibole (~65%), plagioclase (~30%), biotite (~3–4%), magnetite (~1%), and accessory apatite and zircon. It exhibits no clear foliation or lineation, instead having a granoblastic texture. Amphibole forms porphyroblast-like grains that often occur together in larger clusters up to ~10 mm in diameter (Fig. 3a). These grains have Si = 6.19–6.35 pfu (per 23 oxygens), Na + K (A-site) = 0.41–0.57, Na (B-site) = 0.00–0.18, and XMg = Mg/(Mg + Fe²⁺) = 0.70–0.74 (Fig. 5a; Table 2), and are thus tschermakite. Matrix plagioclase forms subhedral grains ~0.1–0.2 mm in diameter and has XCa = Ca/(Ca + Na + K) = 0.51–0.60, and is thus labradorite. Some grains show partial sassuritization (Fig. 3a), possibly due to retrograde fluid-mediated alteration. Magnetite is pure Fe₃O₄ (Fig. 5a; Table 2) and forms anhedral grains that occur adjacent to biotite.

(Fig. 3b). Biotite does not show any preferred orientation and has Ti = 0.54–0.58 pfu (for 22 oxygens) and XMg = 0.54–0.59 (Fig. 5c). There are no measurable halogens in biotite, although tschermakite has ~0.09 pfu F (Table 2).

Trace element ratios for amphibolite sample 17SIMM01 were examined to constrain the initial tectonic setting of formation of its igneous protolith. Discrimination diagrams, shown in the Supplementary Information, indicate that all ratios lie within the island arc tholeiite (IAT) field, indicating that it has a convergent margin geochemical affinity and may have formed as a subaerial or submarine volcanic lava flow in an island arc setting.

Table 1

Bulk-rock major-element oxide (weight % oxide) compositions of all samples. Lithologies collected from the Marion Mine are prefixed 17SIMM and those from Amethyst Prospect are prefixed 17SIAP. Fe₂O₃^{tot} is total iron expressed as Fe₂O₃. LOI = loss on ignition.

Sample	17SIMM01				17SIMM02					17SIMM04					
Lithology	Amphibolite				Garnet–biotite gneiss					Calc-silicate					
Mineral	Bt	Mt	Pl	Ts	Bt	Grt	Ilm	Kfs	Pl	Cal	Chu	Ol	Phl	Sp	Ts
SiO ₂	35.47	0.00	53.19	41.80	34.32	37.06	0.00	63.64	56.88	0.00	36.85	38.59	40.87	0.00	45.56
TiO ₂	4.98	0.00	0.00	0.95	4.26	0.03	45.29	0.21	0.00	0.00	2.90	0.12	0.66	0.00	1.44
ZnO	0.00	0.00	0.00	0.00	0.00	0.00	0.00	0.00	0.00	0.00	0.02	0.00	0.00	14.30	0.03
Al ₂ O ₃	15.21	0.25	29.22	9.86	15.94	21.46	0.04	18.50	26.66	0.00	0.00	0.00	15.04	65.22	11.97
Fe ₂ O ₃	0.34	69.94	0.08	9.32	1.18	2.35	4.27	0.00	0.05	0.00	0.00	0.02	0.43	0.49	0.29
FeO	18.05	31.57	0.00	8.50	19.45	27.62	50.49	0.00	0.00	0.03	4.74	1.39	1.33	4.43	2.76
MnO	0.14	0.00	0.00	0.34	0.22	5.33	0.11	0.01	0.00	0.05	0.46	0.12	0.03	0.15	0.23
MgO	12.48	0.00	0.00	12.06	10.59	4.73	0.07	0.00	0.00	1.32	52.51	60.12	26.50	16.25	20.05
CaO	0.00	0.00	10.98	10.39	0.03	2.22	0.00	0.02	8.38	55.77	0.00	0.00	0.00	0.00	12.09
Na ₂ O	0.06	0.00	5.30	1.42	0.06	0.00	0.00	1.04	6.78	0.00	0.00	0.00	0.84	0.00	1.98
K ₂ O	9.17	0.00	0.18	0.82	9.39	0.02	0.00	14.95	0.24	0.00	0.00	0.00	9.13	0.00	0.45
Cl	0.03	0.00	0.00	0.00	0.10	0.00	0.00	0.00	0.00	0.00	0.00	0.00	0.08	0.00	0.04
F	0.00	0.00	0.00	0.19	0.72	0.00	0.00	0.00	0.00	0.00	2.06	0.00	1.90	0.00	0.79
Total	95.93	101.76	98.95	95.65	96.25	100.82	100.27	98.36	98.99	57.17	99.53	100.36	96.83	100.84	97.67
Si	5.37	0.00	2.43	6.35	5.33	2.99	0.00	2.98	2.58	0.00	3.90	1.00	5.74	0.00	6.47
Ti	0.57	0.00	0.00	0.11	0.50	0.00	0.96	0.00	0.00	0.00	0.23	0.00	0.07	0.00	0.15
Zn	0.00	0.00	0.00	0.00	0.00	0.00	0.00	0.00	0.00	0.00	0.00	0.00	0.00	2.19	0.00
Al	2.71	0.01	1.55	1.77	2.92	2.00	0.00	1.01	1.42	0.00	0.00	0.00	2.49	15.92	2.00
Fe ₃₊	0.04	1.99	0.00	1.07	0.09	0.08	0.06	0.00	0.00	0.00	0.00	0.00	0.03	0.08	0.07
Fe ₂₊	2.28	1.00	0.00	1.08	2.53	1.83	0.97	0.00	0.00	0.00	0.42	0.01	0.16	0.77	0.33
Mn	0.02	0.00	0.00	0.04	0.03	0.36	0.00	0.00	0.00	0.00	0.04	0.00	0.00	0.03	0.03
Mg	2.82	0.00	0.00	2.73	2.45	0.56	0.00	0.00	0.00	0.06	8.28	1.99	5.55	5.02	4.24
Ca	0.00	0.00	0.54	1.69	0.00	0.19	0.00	0.01	0.40	1.93	0.00	0.00	0.00	0.00	1.84
Na	0.02	0.00	0.47	0.42	0.02	0.00	0.00	0.09	0.60	0.00	0.00	0.00	0.23	0.00	0.54
K	1.77	0.00	0.01	0.16	1.86	0.00	0.00	0.90	0.00	0.00	0.00	0.00	1.64	0.00	0.08
Total	15.59	3.00	5.00	15.41	15.73	8.00	2.00	5.00	5.00	2.00	12.87	3.00	15.90	24.00	15.76
Cl	0.00	0.00	0.00	0.00	0.03	0.00	0.00	0.00	0.00	0.00	0.00	0.00	0.02	0.00	0.01
F	0.00	0.00	0.00	0.09	0.36	0.00	0.00	0.00	0.00	0.00	0.69	0.00	0.84	0.00	0.36
OH	2.00	0.00	0.00	1.91	1.62	0.00	0.00	0.00	0.00	0.00	1.31	0.00	1.14	0.00	1.63
Oxygen	22	4	8	23	22	12	3	8	8	3	17	4	22	24	23

Table 2

Representative mineral compositions (wt% oxide and cations per formula unit) from Marion Mine samples. Proportions of Fe₂O₃ and Fe³⁺ were calculated using charge balance.

Sample	17SIAP02						17SIAP04				17SIAP09					
Lithology	Sapphirine hornfels						Marble				Sapphirine hornfels					
Mineral	An	Crn	Phl	Ple	Rt	Spr	Cal	Dol	Fo	Sp	An	Phl	Ple	Prg	Rt	Spr
SiO ₂	42.39	0.00	40.82	0.00	0.00	12.64	0.00	0.00	38.21	0.00	43.42	41.53	0.00	44.81	0.00	12.13
TiO ₂	0.00	0.00	0.52	0.00	97.95	0.00	0.00	0.00	0.12	0.00	0.00	0.57	0.00	0.67	94.36	0.00
ZnO	0.00	0.00	0.00	0.46	0.09	0.00	0.00	0.00	0.00	0.00	0.00	0.00	0.50	0.00	0.00	0.00
Al ₂ O ₃	36.74	100.01	15.21	66.75	0.00	65.02	0.00	0.00	0.00	52.11	36.87	14.95	66.96	15.13	0.00	65.67
Fe ₂ O ₃	0.04	0.00	0.07	1.17	0.00	2.73	0.00	0.00	0.02	18.51	0.00	0.02	0.42	0.16	0.00	2.70
FeO	0.00	0.33	2.64	15.01	0.90	1.80	0.00	0.08	0.39	0.81	0.00	2.74	15.62	4.49	3.87	1.50
MnO	0.00	0.00	0.02	0.12	0.00	0.05	0.05	0.07	0.12	0.20	0.00	0.00	0.09	0.11	0.00	0.08
MgO	0.00	0.00	25.79	17.96	0.00	19.06	1.20	21.36	59.52	24.70	0.00	25.78	17.51	18.04	0.00	18.69
CaO	19.92	0.00	0.00	0.00	0.00	0.02	55.75	29.73	0.00	0.00	19.80	0.00	0.00	12.12	0.00	0.00
Na ₂ O	0.00	0.00	0.93	0.00	0.00	0.00	0.00	0.00	0.00	0.00	0.31	0.93	0.00	1.84	0.00	0.06
K ₂ O	0.02	0.00	8.32	0.00	0.00	0.00	0.02	0.00	0.00	0.00	0.02	8.27	0.00	0.27	0.00	0.00
Cl	0.00	0.00	0.00	0.00	0.00	0.00	0.00	0.00	0.00	0.00	0.00	0.03	0.00	0.00	0.00	0.00
F	0.00	0.00	2.96	0.00	0.00	0.00	0.00	0.00	0.00	0.00	0.00	3.16	0.00	1.20	0.00	0.00
Total	99.11	100.34	97.27	101.47	98.93	101.32	57.02	51.24	98.38	96.33	100.42	97.97	101.11	98.84	98.23	100.83
Si	1.99	0.00	5.75	0.00	0.00	1.46	0.00	0.00	0.97	0.00	2.00	5.81	0.00	6.32	0.00	1.41
Ti	0.00	0.00	0.05	0.00	1.00	0.00	0.00	0.00	0.00	0.00	0.00	0.06	0.00	0.07	0.98	0.00
Zn	0.00	0.00	0.00	0.07	0.00	0.00	0.00	0.00	0.00	0.00	0.00	0.00	0.08	0.00	0.00	0.00
Al	2.02	2.00	2.53	15.82	0.00	8.85	0.00	0.00	0.00	13.04	2.01	2.47	15.94	2.51	0.00	8.97
Fe ³⁺	0.00	0.00	0.00	0.18	0.00	0.24	0.00	0.00	0.00	2.96	0.00	0.00	0.06	0.01	0.00	0.24
Fe ²⁺	0.00	0.00	0.31	2.52	0.00	0.17	0.00	0.00	0.01	0.14	0.00	0.32	2.64	0.53	0.02	0.15
Mn	0.00	0.00	0.00	0.02	0.00	0.01	0.00	0.00	0.00	0.04	0.00	0.00	0.02	0.01	0.00	0.01
Mg	0.00	0.00	5.42	5.39	0.00	3.28	0.06	1.00	2.02	7.82	0.00	5.38	5.27	3.79	0.00	3.23
Ca	1.00	0.00	0.00	0.00	0.00	0.00	1.94	1.00	0.00	0.00	0.98	0.00	0.00	1.83	0.00	0.00
Na	0.00	0.00	0.25	0.00	0.00	0.00	0.00	0.00	0.00	0.00	0.02	0.25	0.00	0.50	0.00	0.01
K	0.00	0.00	1.49	0.00	0.00	0.00	0.00	0.00	0.00	0.00	0.00	1.47	0.00	0.05	0.00	0.00
Total	5.01	2.00	15.81	24.00	1.00	14.00	2.00	2.00	3.01	24.00	5.00	15.76	24.00	15.64	1.00	14.00
Cl	0.00	0.00	0.00	0.00	0.00	0.00	0.00	0.00	0.00	0.00	0.00	0.01	0.00	0.00	0.00	0.00
F	0.00	0.00	1.32	0.00	0.00	0.00	0.00	0.00	0.00	0.00	0.00	1.40	0.00	0.53	0.00	0.00
OH	0.00	0.00	0.68	0.00	0.00	0.00	0.00	0.00	0.00	0.00	0.00	0.59	0.00	1.47	0.00	0.00
Oxygen	8	3	22	18	2	20	3	3	4	18	8	22	18	23	2	20

Table 3

Representative mineral compositions (wt% oxide and cations per formula unit) from Amethyst Prospect samples. Proportions of Fe₂O₃ and Fe³⁺ were calculated using charge balance.

Sample no.	Lithology	SiO ₂	Al ₂ O ₃	Fe ₂ O ₃ (T)	MnO	MgO	CaO	Na ₂ O	K ₂ O	TiO ₂	LOI	Total
17SIMM01	Amphibolite	46.47	16.66	12.97	0.22	7.08	10.57	2.81	0.75	0.90	0.83	99.26
17SIMM02	Garnet-biotite gneiss	74.33	11.95	3.81	0.10	1.60	3.13	2.42	1.43	0.53	0.75	100.05
17SIMM04	Calc-silicate	32.85	17.13	7.46	0.35	25.07	2.94	0.34	0.34	0.79	3.55	90.82
17SIAP02	Sapphirine hornfels	29.39	34.41	6.09	0.06	17.31	3.50	0.53	3.16	0.54	3.76	98.75
17SIAP04	Marble	9.38	1.61	2.40	0.13	20.67	31.50	0.01	< 0.01	0.02	32.32	98.04
17SIAP09	Sapphirine hornfels	29.62	34.09	6.04	0.06	17.43	3.60	0.55	3.38	0.57	3.59	98.93

3.3.2. 17SIMM02 – Garnet–biotite gneiss

Sample 17SIMM02 contains biotite (~9–10%), garnet (~1–2%), plagioclase (~45%), K-feldspar (~5%), quartz (~40%), ilmenite (~1%) and accessory monazite, apatite, and zircon. It contains centimeter-scale leucosome segregations (Fig. 3c) interlayered with biotite-rich melanosome domains. Garnet occurs only in leucosomes forms as porphyroblasts up to ~10 mm in diameter that are partially replaced by biotite at their rims (Fig. 3c). Analysis of core and rim domains shows a lack of internal zoning, with a composition $\text{Alm}_{0.63}\text{Prp}_{0.14}\text{Sps}_{0.13}\text{Grs}_{0.07}$ (Table 2), where Alm = almandine = $\text{Fe}^{2+}/(\text{Fe}^{2+} + \text{Mg} + \text{Ca} + \text{Mn})$, Prp = pyrope = $\text{Mg}/(\text{Fe}^{2+} + \text{Mg} + \text{Ca} + \text{Mn})$, Grs = grossular = $\text{Ca}/(\text{Fe}^{2+} + \text{Mg} + \text{Ca} + \text{Mn})$, and Sps = spessartine = $\text{Mn}/(\text{Fe}^{2+} + \text{Mg} + \text{Ca} + \text{Mn})$. Such profiles are typical of grains that have experienced intracrystalline diffusional relaxation of compositional gradients acquired during growth. Leucosome plagioclase forms subhedral grains ~0.1–0.2 mm in diameter and has $X_{\text{Ca}} = 0.34\text{--}0.41$, and K-feldspar has $X_{\text{Na}} = \text{Na}/(\text{Na} + \text{K}) = 0.06\text{--}0.11$ (Table 2). Melanosome biotite grains have similar compositions to leucosome grains, with Ti = 0.46–0.50 pfu (for 22 oxygens), XMg = 0.49–0.51, and Cl = 0.02–0.03 pfu and F = 0.30–0.42 pfu (Fig. 5c; Table 2).

3.3.3. 17SIMM04 – Calc-silicate

Sample 17SIMM04 is a strongly mineralized calc-silicate containing calcite and dolomite, having a combined volume proportion of ~30%, olivine (~5%), spinel (~15%), clin amphibole (~10%), quartz (~20%), galena (~15%), and chalcopyrite and pyrite (~5%). Clinohumite is rare, but contains ~2 wt% F (Table 2). The sample has a hornfelsic texture with no foliation or lineation (Fig. 3d). Olivine has an XMg = 0.93–0.97 (Table 2), indicating that it is forsterite, and occurs as anhedral grains ~2–5 mm in diameter. Most grains contain chlorite and serpentine in fractures (Fig. 3e). Amphibole occurs in the matrix and has Si = 6.33–6.95 pfu (for a 23-oxygen calculation), Na + K (A-site) = 0.43–0.67 and XMg = 0.97–1.00 (Fig. 5a; Table 2), and is thus pargasite. These amphiboles also contain Cl = 0.01 pfu and F = 0.34–0.42 pfu (Table 2). Biotite has XMg = 0.97–0.98, Ti = 0.03–0.04 pfu, Cl = 0.02 pfu, and F = 0.84–0.93 pfu, making the grains extremely halogen-rich phlogopite (cf. Fig. 5c). Abundant spinel grains have XMg = 0.84–0.87 and $X_{\text{Fe}^{3+}} = \text{Fe}^{3+}/(\text{Al} + \text{Fe}^{3+}) < 0.01$ (Fig. 5b). Additionally, they contain ~14 wt% ZnO (~2.2 cpfu for a 24-oxygen calculation: Table 2), indicating solid solution towards the gahnite end member.

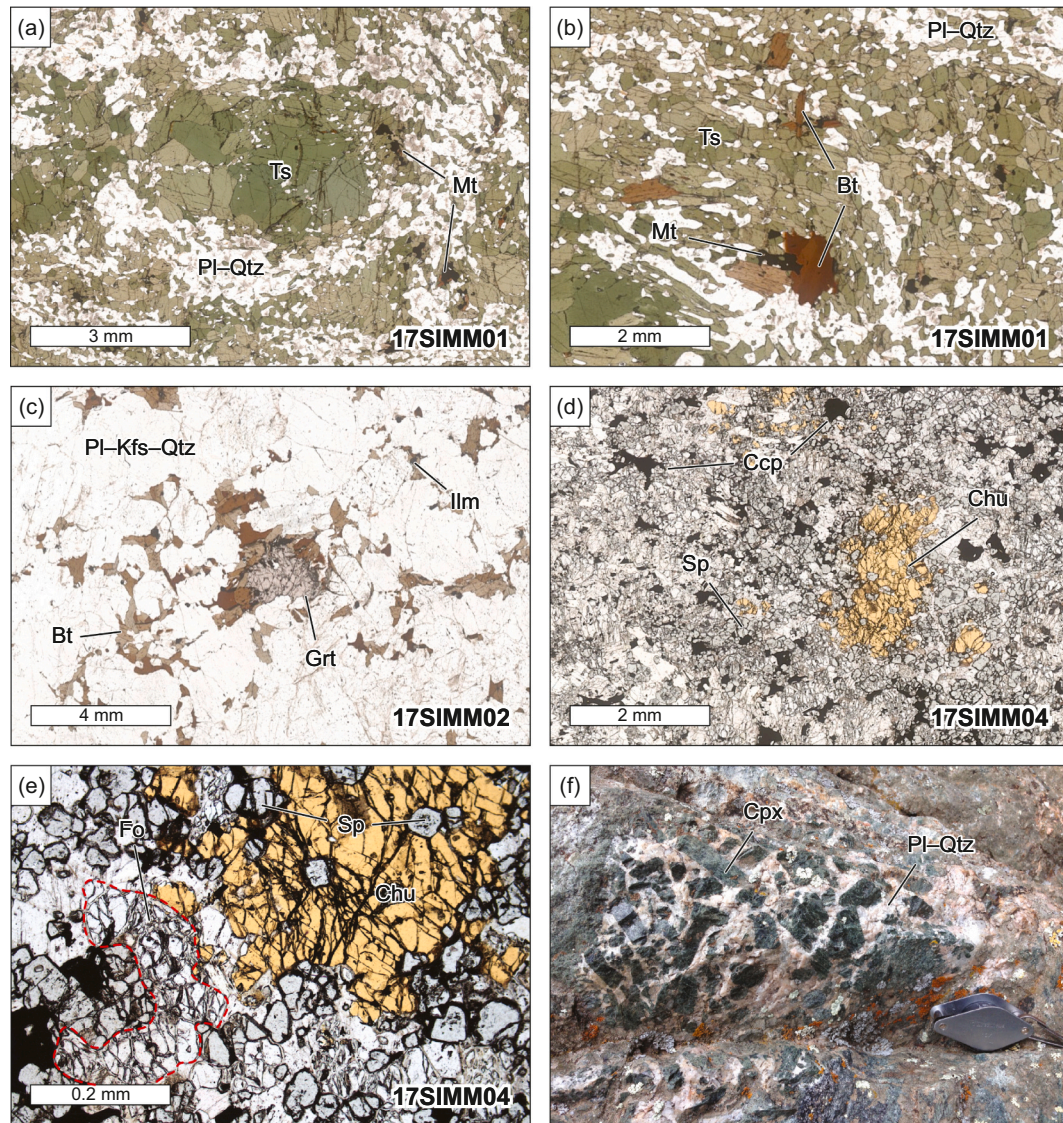


Fig. 3. Petrological features in Marion Mine samples. (a) Amphibolite 17SIMM01 with tschermakite aggregates surrounded by a plagioclase–quartz matrix and (b) large, undeformed biotite grains. (c) Leucosome 17SIMM02 containing anhedronal garnets surrounded by biotite, quartz, and plagioclase. (d) Calc-silicate 17SIMM04 dominated by carbonate and zirconian spinel, with subhedral clinohumite poikiloblasts and accessory chalcopyrite. (e) Detail of clinohumite poikiloblast containing inclusions of spinel and adjacent to matrix olivine, which is weakly serpentinized. (f) Field photograph showing a clinopyroxene-rich leucocratic segregation adjacent to an adit in the Marion Mine. Hand lens for scale.

3.4. Amethyst Prospect

Lithologies collected from the Amethyst Prospect include sapphirine-bearing hornfels, calc-silicate gneiss, marble, and garnet–cordierite gneiss.

3.4.1. 17SIAP02 – Sapphirine hornfels

Sample 17SIAP02 is a sapphirine-bearing hornfels containing spinel (~20%), phlogopite (~55%), plagioclase (~20%), corundum (~3%), sapphirine (~2%), and accessory monazite, rutile, and zircon. Akin to Marion Mine samples, it contains no dominant foliation or lineation, despite the abundance of mica (Fig. 4a). Spinel is abundant and typically forms clusters up to ~15 mm in diameter. It has $X_{Mg} = 0.66–0.71$ and $X_{Fe^{3+}} = Fe^{3+}/(Al + Fe^{3+}) = 0.01$, being compositionally classified as pleonast (Fig. 5b). It also contains negligible Zn (~0.06 cpfu for a 24-oxygen calculation; Table 3). Plagioclase occurs in randomly distributed patches of euhedral to subhedral grains ~0.1–0.2 mm in diameter, and has $X_{Ca} = 0.98$, and thus is anorthite (Table 3). Biotite is almost completely colorless in thin section, does not show any preferred

orientation, and has $Ti = 0.04–0.08$ apfu, $X_{Mg} = 0.95$, and $F = 1.26–1.39$ apfu for a 22-oxygen calculation (Fig. 5c; Table 3), compositionally classifying it as a halogen-rich phlogopite. These grains also contain minor Na (0.2–0.3 pfu; Fig. 5c). Corundum is pure Al_2O_3 with no measurable impurities and forms subhedral grains ~1–2 mm in diameter that are ubiquitously surrounded by coronae of pleonast (Fig. 4a). Sapphirine has $Al = 8.79–9.43$ cpfu (for 20 oxygens) and $Mg = 3.02–3.30$ pfu (Table 3), and occurs as small nodules in clear textural equilibrium with spinel, phlogopite, and anorthite (Fig. 4b). These sapphirine compositions lie close to the ideal 7:9:3 end-member (Fig. 5d; Grew et al., 2008). Notably, sample 17SIAP02 lacks quartz, which would otherwise be an indicator of UHT metamorphism if both minerals existed in mutual equilibrium.

3.4.2. 17SIAP04 – Marble

Sample 17SIAP04 is an isotropic marble comprised of calcite and dolomite (~75%), olivine (~20%), and spinel (~5%). Trace amounts of magnetite, quartz, chalcopyrite and pyrite occur in the matrix (Fig. 4c). Olivine occurs as euhedral, rounded grains and has $X_{Mg} = 0.99–1.00$,

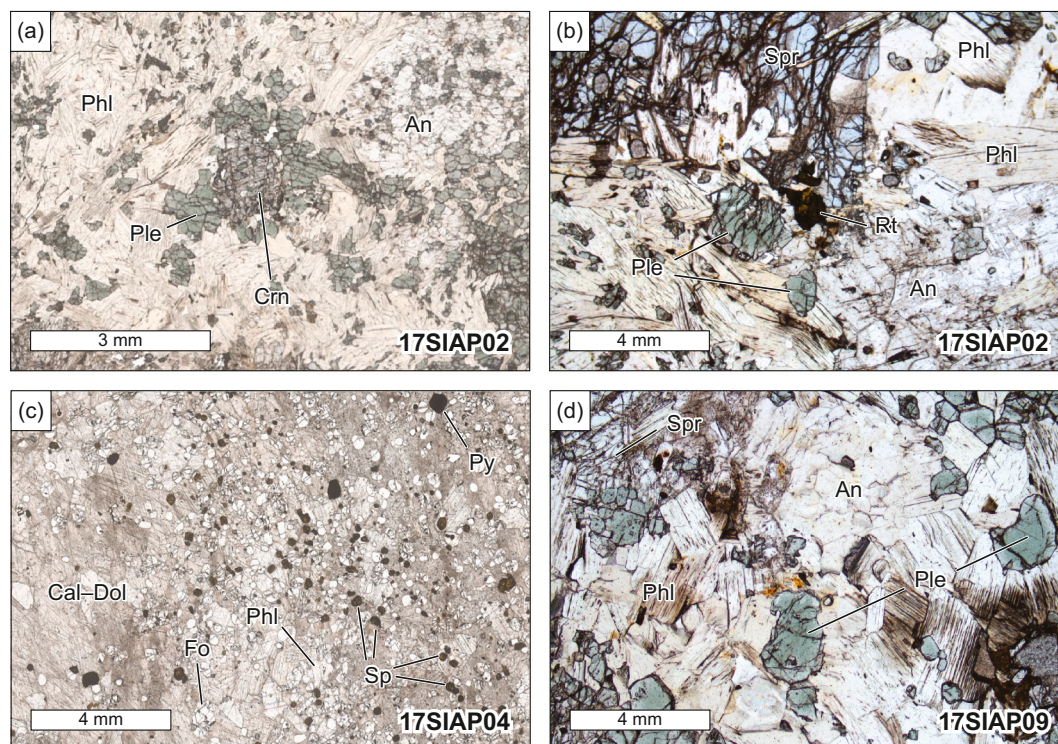


Fig. 4. Petrological features in Amethyst Prospect samples. (a) Sapphirine hornfels 17SIAP02 containing corundum porphyroblasts rimmed by green pleonast. Patches of coarse and randomly oriented anorthite occur within the matrix, which is dominated by phlogopite. (b) Sapphirine in textural equilibrium with rutile, phlogopite, and anorthite. (c) Marble 17SIAP04 containing abundant olivine and spinel. Accessory pyrite also occurs. (d) Sapphirine hornfels 17SIAP09 with a similar paragenesis to 17SIAP02. (For interpretation of the references to colour in this figure legend, the reader is referred to the web version of this article.)

making it forsterite (Table 3). These grains are often highly fractured, but show no hydrous alteration. Spinel is golden yellow in colour and has $XMg = 0.97\text{--}0.98$ and $XFe^{3+} = 0.14\text{--}0.18$ (Fig. 5b). It contains no measurable Zn (Table 3).

3.4.3. 17SIAP09 – Sapphirine hornfels

Sample 17SIAP09 is petrologically similar to 17SIAP02, but contains additional galena and minor amphibole (~5%), which is accounted for by lesser phlogopite. The amphibole grains have $Si = 6.25\text{--}6.32$ cpfu, $(Na + K)$ in the A site = $0.50\text{--}0.54$, and $XMg = 0.95\text{--}0.96$, so are paragonite (Fig. 5a). They contain negligible Cl (<0.01 pfu) but have an F content of $0.46\text{--}0.54$ pfu (per 23 oxygens: Table 3). All other minerals and microstructures are the same as those described for sample 17SIAP02 (cf. Fig. 4d).

4. U–Pb monazite geochronology

Radiogenic isotope geochronology was performed on samples collected from both Marion Mine and Amethyst Prospect localities in order to determine the age of metamorphism in this part of the southern Wet Mountains. Monazite was focused upon, as it is a common accessory mineral in metaluminous and peraluminous metapelitic rocks, preferentially incorporates high concentrations of Th and U, and has very low initial concentrations of common Pb (Aleinikoff et al., 2006). It is also extremely resistant to U–Th–Pb internal diffusion at temperatures $<900^\circ\text{C}$, which can allow successive phases of growth to be recorded in rocks that have undergone multiple tectonic or metamorphic episodes. Abundant monazite was identified in sapphirine hornfels samples 17SIAP02 and 17SIAP09 and leucosomes in garnet–biotite gneiss sample 17SIMM02, although none was present in amphibolite sample 17SIMM01, calc-silicate sample 17SIMM04, or marble sample 17SIAP04.

4.1. Analytical conditions

All isotopic data were collected in-situ to provide textural context to the ages obtained using laser-ablation inductively coupled plasma mass spectrometry (LA-ICP-MS) at the USGS Crustal Geophysics and Geochemistry Science Center in Denver, Colorado, U.S.A. Detailed analytical procedures are given in the Supplementary Information. All U–Pb sample data were interpreted graphically on Wetherill diagrams produced using the MS Excel add-in Isoplot. All ellipses on these plots and uncertainties are given at the 2σ level, and all U–Pb geochronological data are given in Table S1.

4.2. Results

Monazite in garnet–biotite gneiss leucosome (17SIMM02) is anhedral, around $20\text{--}50\text{ }\mu\text{m}$ in diameter, and exhibits no internal zoning in backscattered electron (BSE) images. Twenty-seven spot analyses were obtained from nine different grains, although six data points were discarded due to having poor ablation profiles during analysis. All remaining data ($n = 21$) were interpreted as a single concordant population that has a U–Pb age of 1346.9 ± 6.9 Ma (Fig. 6a; MSWD = 4.5).

Monazite in sapphirine hornfels sample 17SIAP02 occurs exclusively within the matrix as anhedral grains, $30\text{--}60\text{ }\mu\text{m}$ in diameter, and which exhibit no internal zoning in BSE images. Thirty-eight spot analyses were obtained from twelve different grains throughout the sample, although 15 were discarded due to either having poor ablation profiles or very high concentrations of common lead. Of the remaining 23 spot analyses, 17 lie close to concordia and can be interpreted to lie along a single chord with a U–Pb lower-intercept age of 1321 ± 25 Ma (Fig. 6b; MSWD = 1.5).

Monazite in sapphirine hornfels sample 17SIAP09 is generally anhedral to euhedral, $40\text{--}60\text{ }\mu\text{m}$ in diameter, and mostly exhibits no internal zoning in BSE images. Many show equilibrium microstructures

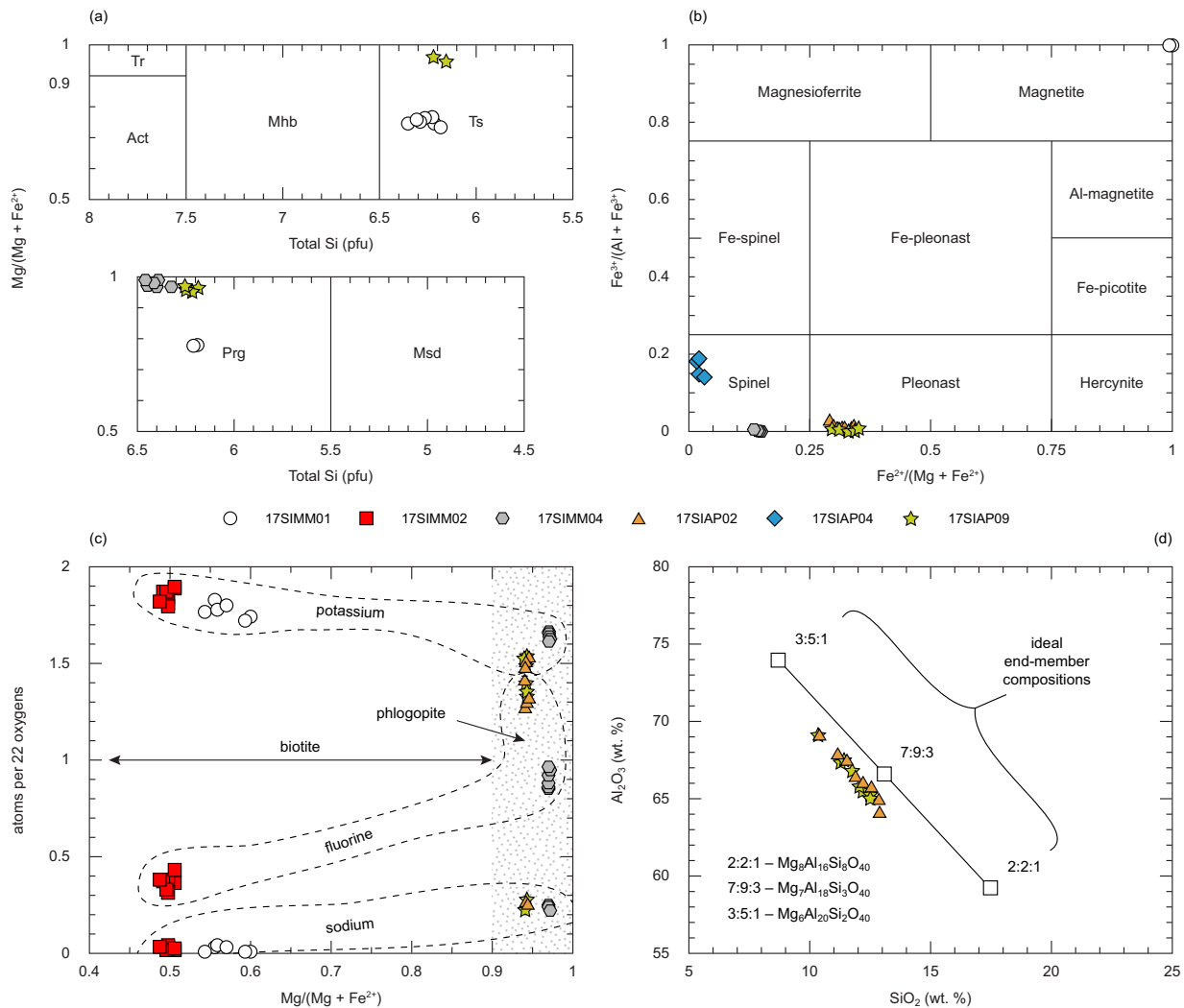


Fig. 5. Mineral compositions from all samples. (a) Amphibole classification plot showing Si atoms per formula unit and $\text{Mg}/(\text{Fe}^{2+} + \text{Mg})$. The top grid refers to group-2 calcic amphiboles with (Na + K) in the A site < 0.5 , and the bottom grid refers to group-2 calcic amphiboles with (Na + K) in the A site > 0.5 . (b) Spinel-group classification plot (after Bosi et al., 2018) in terms of $\text{Fe}^{2+}/(\text{Mg} + \text{Fe}^{2+})$ and $\text{Fe}^{3+}/(\text{Al} + \text{Fe}^{3+})$. (c) Biotite compositional parameters showing K, Na, and F atoms per formula unit versus $\text{Mg}/(\text{Fe}^{2+} + \text{Mg})$. Phlogopite is defined as having $\text{Mg}/(\text{Fe}^{2+} + \text{Mg}) > 0.9$. (d) Sapphirine classification plot (after Grew et al., 2008) in terms of weight percent Al_2O_3 and SiO_2 . Ideal compositions for 2:2:1, 7:9:3, and 3:5:1 end-members are shown for reference.

with the peak mineral assemblage, as shown in Fig. 6c in the inset, where a monazite grain within a spinel aggregate exhibits equilibrium $\sim 120^\circ$ grain boundary intersections. Thirty-eight spot analyses were obtained from nine different grains throughout the sample, although 11 were discarded due to having poor ablation profiles. The remaining data show various degrees of discordance, akin to sample 17SIAP02, with a cluster of 14 lying close to concordia. These data are interpreted using a single chord that has a U-Pb lower-intercept age of 1342 ± 16 Ma (Fig. 6d; MSWD = 1.12; $n = 14$). Together, these age data constrain the timing of metamorphism in both localities to c. 1340–1320 Ma, which slightly post-dates the age of crystallization reported for the San Isabel granite (1362 ± 7 Ma, U-Pb zircon: Bickford et al., 1989). This age range also post-dates the timing of amphibolite-facies metamorphism of other metasediments and meta-igneous rocks in the southern Wet Mountains that lie far away from the San Isabel granite, such as the Williams Creek amphibolite (c. 1430 Ma: Fig. 2a).

5. Thermobarometry

Constraining the P – T conditions at which the country rocks around the San Isabel granite equilibrated is critical to supporting

interpretations of whether they preserve regional metamorphic assemblages related to orogenic deformation or localized contact metamorphic assemblages that formed in response to magmatic intrusion. Both phase diagram-based petrological modeling and conventional thermobarometry were employed, as each technique provides independent estimations of P – T conditions for making tectonic interpretations, but each also has caveats and uncertainties (Palin et al., 2016a). Setup conditions and model parameters for petrological modeling of each individual sample are described in the Supplementary Information.

5.1. Petrological modeling

5.1.1. 17SIMM01 – Amphibolite

A pseudosection for 17SIMM01 calculated at P – T conditions of 2–10 kbar and 600–900 °C is shown in Fig. 7a. The phase equilibria correlate well with those predicted for metamorphosed mid-ocean ridge basalt (MORB) and similar mafic precursor lithologies at amphibolite- and granulite-facies conditions (cf. Diener et al., 2007; Palin et al., 2016c), although sample 17SIMM01 is slightly less titaniferous than these generic lithologies, which suppresses the stabilization of ilmenite and

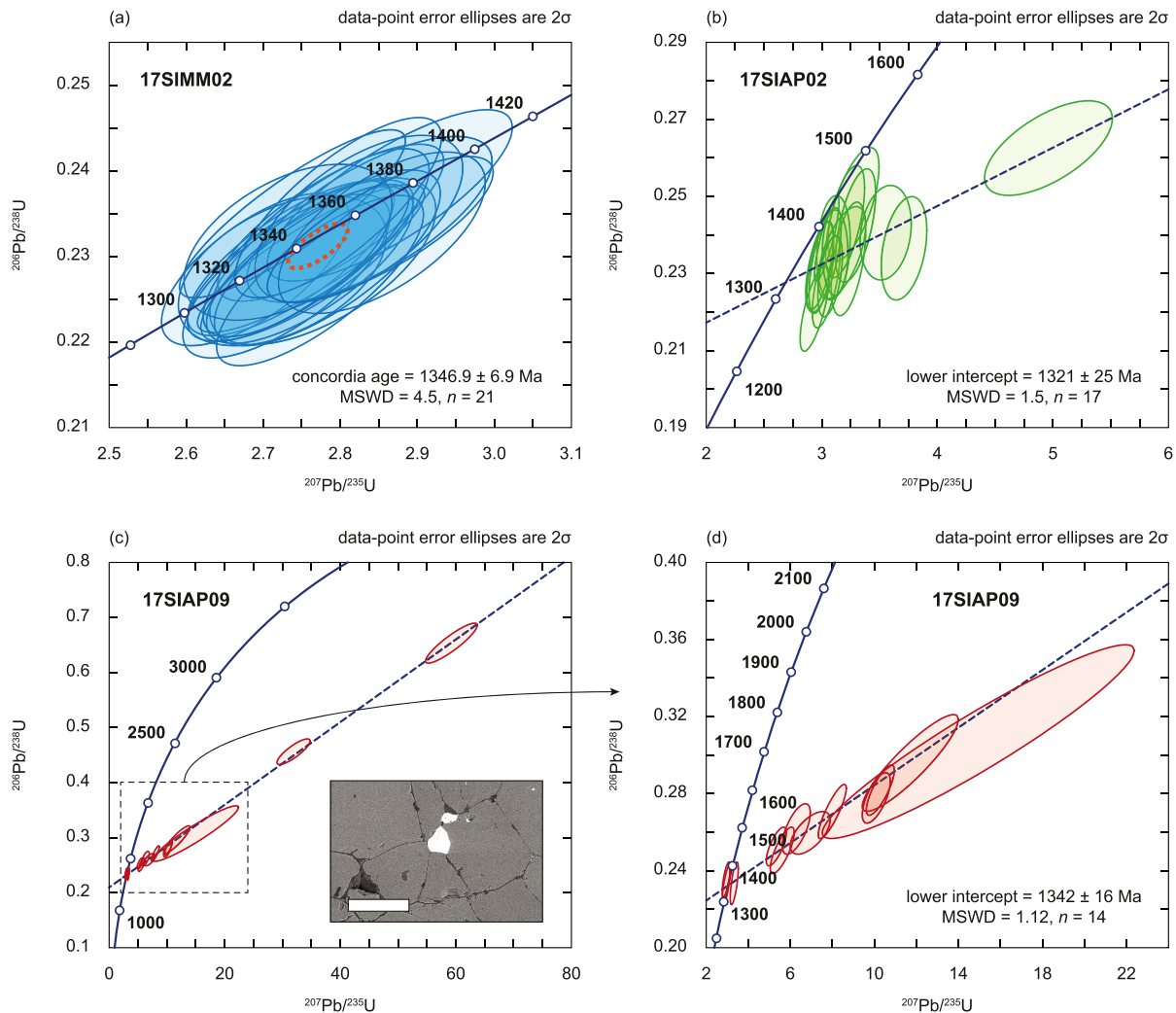


Fig. 6. Wetherill plots showing the results of U-Pb monazite geochronology for samples (a) 17SIMM02, (b) 17SIAP02, and (c) 17SIAP09. Inset in part (c) shows a BSE image of a monazite grain within a spinel cluster. White bar equals 100 μm . (d) Detailed view of data for 17SIAP09 excluding two highly discordant analyses.

rutile at $T > 750$ °C. The fluid-saturated solidus for 17SIMM01 nadirs at ~ 680 °C at ~ 6.5 kbar and contours showing the volume proportion of partial melt are shown by dashed lines (Fig. 7a). Calcic amphibole (hornblende, *sensu lato*) and plagioclase are stable across the P – T range of interest, and garnet is stable at $P > 8$ kbar.

The observed mineral assemblage in sample 17SIMM01 of tschermakite, plagioclase, biotite, and magnetite (Fig. 3a) is not calculated to be stable anywhere within the P – T field of interest, owing in part to the predicted stability of augitic clinopyroxene at both subsolidus and suprasolidus conditions. No clinopyroxene was observed in sample 17SIMM01 or has been reported by other workers from meta-mafic rocks in the Wet Mountains (Levine et al., 2013); however, the calculated proportion of augite in this model is ~ 2 –5 vol% at subsolidus conditions and rises to ~ 14 vol% at 900 °C and 8–10 kbar at high-pressure granulite facies conditions. This issue is problematic for phase diagram-based thermobarometry, as it is unlikely that minerals with proportions exceeding ~ 1 –2 vol% would be missed during thin section inspection. This discrepancy can be accounted for by the over-stabilization of augite in petrological models at amphibolite-facies conditions (cf. Forshaw et al., 2019). In addition, where stable at the correct P – T conditions, the calculated Mg and Si contents of clinopyroxene are generally underestimated compared to natural grains, while Fe^{2+} and Al are typically overestimated. As such, the occurrence of minor augite in the calculated P – T pseudosection for 17SIMM01

(Fig. 7a) can be overlooked as an artifact of imprecisions in the calibration of the a – x relation of Green et al. (2016).

A further complexity related to the calculated phase equilibria for sample 17SIMM01 is the presence of partial melt at $T > 650$ °C, where there is no clear evidence for anatexis at the hand sample or thin section scale. Although coarse clusters of amphibole appear to be mantled by quartz–plagioclase aggregates (Fig. 3a), these leucocratic segregations lack diagnostic features of incipient partial melting at grain boundaries, such as recrystallized melt films or the growth of peritectic mafic porphyroblasts (Sawyer, 1999). However, an upper limit to the temperature of peak metamorphism may be inferred by the presence of minor biotite in sample 17SIMM01, which destabilizes at ~ 800 – 825 °C in this model (Fig. 7a). The proportion of melt predicted to be stable at these conditions is no greater than 10 vol%, which is less than the limit for melt connectivity and escape in metamafic rocks. Partial melts generated at upper amphibolite facies conditions in metabasites are tonalitic in composition (Ellis and Thompson, 1986; Palin et al., 2016b). As such, it is possible that incipient partial melting did occur in sample 17SIMM01 during metamorphism, but melt was unable to percolate out from the local environment, such that it recrystallized in-situ to form quartz- and plagioclase-rich segregations observed in thin section (Fig. 3a).

Alongside these factors, the presence of minor F within pargasitic amphibole in 17SIMM01 (0.09 pfu; Table 2) places limitations on the reliability of phase equilibria calculated in halogen-absent

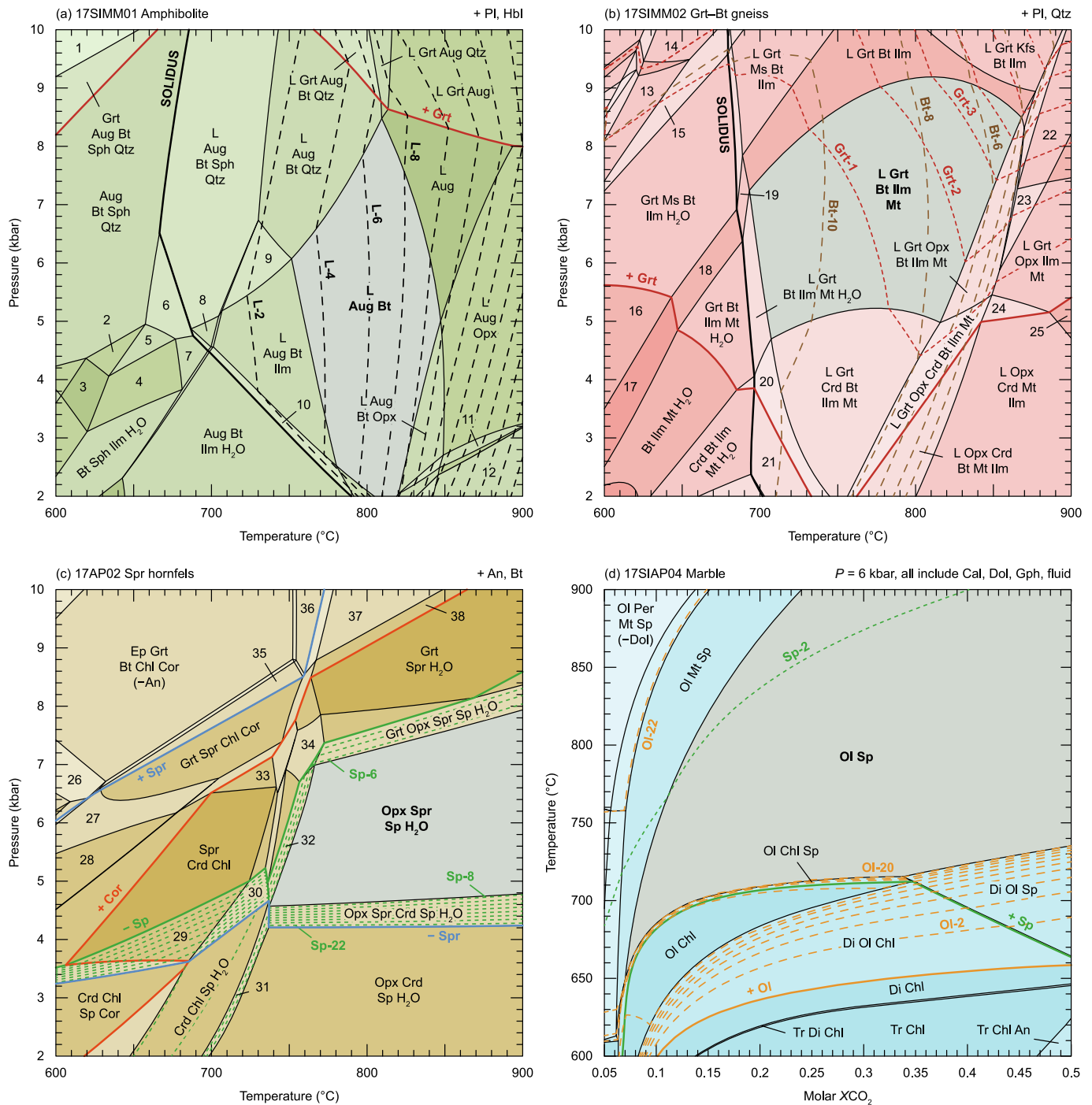


Fig. 7. Calculated P - T pseudosections for samples (a) 17SIMM01, (b) 17SIMM02, (c) 17SIAP02, and (d) 17SIAP04. Bulk compositions used for modeling are given in Table 4. Calculated contours showing the proportion of key phases are shown by dashed lines labeled with the phase abbreviation and the calculated vol% of the solid assemblage. Numbered assemblages are documented in the Supplementary Information.

compositional systems. The presence of F in amphibole in sample 17SIMM01 requires aqueous fluid in equilibrium with this mineral paragenesis during metamorphism to have an activity less than unity, which suppresses the onset of melting to higher temperatures (Arano-vich et al., 2013). With these factors in mind, we suggest that conditions of around 770–820 °C at middle crustal pressures are representative of peak metamorphism for sample 17SIMM01, represented here by the calculated assemblage field L-Aug-Bt-Pl-Hbl (Fig. 7a), although uncertainty on these values remains high.

5.1.2. 17SIMM02 – Garnet–biotite gneiss

A pseudosection for 17SIMM02 is shown in Fig. 7b calculated at the same P - T conditions as sample 17SIMM01, which encompass the conditions expected in orogenic belts and high-temperature metamorphic aureoles around felsic intrusions. The phase equilibria resemble those expected in a low- Al_2O_3 metapelite (Palin and Dyck, 2021; White et al., 2014), with the fluid-saturated solidus marking the onset of partial melting at ~670 °C. Garnet is stable across most of the P - T range, with its presence at the onset of melting requiring a minimum pressure of ~4 kbar (Fig. 7b). The interpreted peak metamorphic assemblage in 17SIMM02 (Grt-Bt-Ilm-Kfs-Pl-Qtz-melt) is calculated to be stable at

P - T conditions of ~ 700 – 840 °C and ~ 5 – 9 kbar, with additional minor magnetite. This P - T range is limited at lower pressure by the stabilization of cordierite, at low temperature by the solidus, and at high temperature by the formation of orthopyroxene at the expense of biotite (Fig. 7b). Further refinement of likely metamorphic P - T conditions in this assemblage field can be determined by comparing observed and calculated proportions of garnet and biotite. In 17SIMM02, garnet comprises ~ 1 – 2 vol% and biotite comprises ~ 9 – 10 vol%, suggesting conditions of equilibration at the low temperature (~ 750 °C) and intermediate pressure (~ 5 – 7 kbar) part of this range. These conditions overlap with those inferred for peak metamorphism in sample 17SIMM01 (Fig. 7a).

5.1.3. 17SIAP02 – Sapphirine hornfels

Calculated equilibria for 17SIAP02 are shown in Fig. 7c for the same P - T range considered for samples 17SIMM01 and 17SIMM02. Biotite (phlogopite: $X_{Mg} = 0.91$ – 0.96) is stable throughout this range and anorthite is stable in all fields excluding at low- T and high- P conditions, where epidote is stable instead. For this modeled bulk composition (Table 4), corundum is restricted to nominally low-grade conditions, as delimited by the bold red line shown on Fig. 7c. Sapphirine is stable at pressures above 3–4 kbar, whereas spinel is restricted to pressures below 5 kbar at $T < 750$ °C and 7–8 kbar at higher grade (Fig. 7c). Partial melting is not predicted for this bulk composition, despite the high measured fluid content (Table 1: 3.76 wt%).

The major mineral assemblage observed in sample 17SIAP02 (Spr–Sp–An–Phl–Cor) does not occur as a stable paragenesis on the calculated pseudosection (Fig. 7c), fundamentally due to the low-grade stability of corundum and the high-grade stability of spinel. Corona-like microstructures showing spinel (pleonast) separating corundum from the matrix assemblage (Fig. 4a) indicate that the latter phase was likely not part of the peak assemblage, whereas spinel, sapphirine, anorthite, and phlogopite are observed to be in textural equilibrium (Fig. 4b). As such, corundum may be interpreted as an early-formed mineral that was partially replaced during prograde metamorphism or else a peak metamorphic mineral that formed a corona of spinel during retrograde cooling. However, the phase topologies and calculated stability of corundum at low temperatures (Fig. 7c) indicate that the former interpretation is more likely.

Calculated phase assemblages containing sapphirine, spinel, anorthite, and phlogopite occur at ~ 4 – 8 kbar at $T > 750$ °C, and are limited at low pressure by the breakdown of sapphirine to form cordierite and at high pressure by the breakdown of spinel to form garnet. All such assemblages are also calculated to coexist with either chlorite (clinochlore) at $T < 750$ °C or orthopyroxene (enstatite) at higher temperatures (Fig. 7c). This inability to correctly match the observed peak paragenesis with an equivalent assemblage on this pseudosection again limits the reliability of estimates of peak P - T conditions of metamorphism, although methodological limitations can be invoked to account for this problem. Phlogopite in sample 17SIAP02 is unusually F rich (1.32 pfu; Table 3), whereas the current generation of a - x relations for biotite mica does not permit halogens to substitute for OH[−] (White et al., 2014). As such, the calculated proportion of phlogopite may be significantly underestimated, which affects the proportion of other key

components (e.g. FeO, MgO) available for coexisting phases to satisfy mass balance constraints. The calculated stabilization of ~ 15 vol% orthopyroxene at high-grade conditions, which was not observed in sample 17SIAP02, may be a result of this issue.

Based on the relative stability fields of the major minerals observed within 17SIAP02, the calculated assemblage Opx–Spr–Sp–An–Bt–H₂O is interpreted to best approximate peak metamorphism for this sample (Fig. 7c), which is supported in part by the similarity in P - T conditions with those interpreted for 17SIMM01 and 17SIMM02. This assemblage field is not constrained at high temperature within the P - T range considered, which we do not extend to true UHT conditions due to the absence of supporting petrological or field evidence for such extreme thermal metamorphism.

5.1.4. 17SIAP04 – Marble

The calculated T - X_{CO_2} pseudosection for sample 17SIAP04 is shown in Fig. 7d and demonstrates that all assemblages coexist with calcite, dolomite, graphite, and aqueous fluid. At moderate X_{CO_2} values, clinochlore and tremolite stabilize at low-temperature conditions (< 625 °C), whereas diopside forms at $T \sim 625$ – 710 °C. Olivine (forsterite) and spinel form at higher grade conditions, although the absolute temperature of stabilization of each varies according to fluid composition. The interpreted peak assemblage of olivine, spinel, calcite, and dolomite (Fig. 4c) is calculated to be stable at a temperature as low as ~ 650 °C at very low X_{CO_2} values (~ 0.06), but levels off at ~ 700 – 720 °C when in equilibrium with a more carbon-rich fluid ($X_{CO_2} > 0.10$). At fluid X_{CO_2} values above 0.35, the low-temperature limit of this assemblage is constrained by the stabilization of diopside, which was not observed in this sample. This peak assemblage is also constrained to low fluid X_{CO_2} values at high temperature by the stabilization of magnetite, periclase, and loss of dolomite (Fig. 7d).

Neither the composition of metamorphic fluid in equilibrium with the solid assemblage at peak conditions nor the approximate temperature of metamorphism can be constrained further by examination of changing volume proportions of major phases, as little variation occurs across the field of interest (Fig. 7d). The observed proportions of olivine (20 vol%) matches the calculated proportion in this interpreted peak assemblage field, although the observed proportion of spinel (5 vol%) exceeds the calculated value of 1–2 vol%. However, given the absence of chlorite and/or diopside in this sample, we take the low-temperature limit of ~ 700 °C for this peak assemblage to represent a minimum value for metamorphism, which overlaps with that suggested for all other samples.

5.2. Conventional thermobarometry and P - T synthesis

Pseudosection analysis fundamentally relies upon definition of an effective bulk composition within which all phases are in mutual chemical equilibrium; however, corona-like structures in 17SIAP02 and the presence of partial melting in 17SIMM02 suggest that this assumption may be partly violated in these cases. An alternative technique for investigating the P - T conditions of metamorphism is conventional thermobarometry, which relies only on chemical equilibrium having been reached between the phases of interest, which themselves may

Table 4

Bulk-rock compositions used for phase diagram construction (mole % oxide). FeO^{tot} is total iron expressed as FeO. O is oxygen, which combines with FeO via the equation $2FeO + O = Fe_2O_3$; hence, bulk O is equal to bulk Fe_2O_3 , while true bulk FeO is given by $FeO^{tot} - 2 \times O$. Bulk-rock $X_{Mg} = MgO/(MgO + FeO^{tot})$ and $X_{Fe3+} = (2 \times O)/FeO^{tot}$.

Sample	Lithology	Fig.	H ₂ O	SiO ₂	Al ₂ O ₃	CaO	MgO	FeO _{tot}	K ₂ O	Na ₂ O	TiO ₂	MnO	O	CO ₂	X_{Mg}	X_{Fe3+}
17SIMM01	Amphibolite	7a	4.79	47.28	9.99	11.38	10.74	11.04	0.49	2.77	0.69	–	0.86	–	0.49	0.15
17SIMM02	Garnet–biotite gneiss	7b	2.59	76.99	7.29	3.33	2.47	3.30	0.94	2.43	0.42	0.09	0.15	–	0.43	0.09
17SIAP02	Sapphirine hornfels	7c	12.55	29.40	20.29	3.72	25.81	5.10	2.02	–	–	–	0.15	–	0.84	0.06
17SIAP04	Marble ($X_{CO_2} = 0.05$)	7d	19.00	9.75	0.99	35.06	32.02	2.09	–	–	–	–	0.11	1.00	0.94	0.10
	Marble ($X_{CO_2} = 0.5$)	7d	10.00	9.75	0.99	35.06	32.02	2.09	–	–	–	–	0.11	10.00	0.94	0.10

exist within a smaller equilibrium domain than the rock itself.

An alternative constraint on the minimum temperatures of metamorphism reached in the study region was made by applying the Ti-in-biotite thermometer of Henry et al. (2005). Values obtained via this calibration typically represent minima owing to the possibility of Ti-undersaturation in the effective bulk composition at the time of biotite formation, which is difficult to verify in the absence of saturating Ti-bearing accessory minerals. Alternatively, calculated temperatures that show a range of values may represent ‘true’ temperatures that spread between peak metamorphic conditions and points on the retrograde cooling path, where biotite grains variably reequilibrate down-temperature with adjacent matrix phases and change their compositions accordingly (Frost and Chacko, 1989). The precision on this thermometer varies based on temperature, with 1-sigma uncertainty of $\pm 24^\circ\text{C}$ at greenschist facies and $\pm 12^\circ\text{C}$ at amphibolite facies and above (Henry et al., 2005).

The Ti contents and XMg values of biotite analyzed in samples from the San Isabel granite aureole are shown in Fig. 8a alongside isotherms with a 10°C interval calculated using the calibration of Henry et al. (2005). Biotite in each sample shows negligible compositional variation, such that all data groups are tightly clustered. The most Fe-rich grains were observed in amphibolite sample 17SIMM01 and suggest temperatures of equilibration of $\sim 730\text{--}745^\circ\text{C}$, although the absence of a Ti-oxide in the matrix of this rock suggests the probability of Ti-undersaturation. By contrast, biotite grains in 17SIMM02 leucosome are likely to be Ti-saturated owing to the presence of ilmenite, and suggest temperatures of crystallization of $760\text{--}780^\circ\text{C}$ (Fig. 8a). High-Mg phlogopite grains in both sapphirine-bearing hornfels samples 17SIAP02 and 17SIAP09 are Ti-poor ($\sim 0.04\text{--}0.08$ per 22 oxygens) and show interpreted temperature ranges of crystallization of $\sim 500\text{--}640^\circ\text{C}$, which is only slightly lower than the temperature range suggested for phlogopite in marble 17SIAP04 ($\sim 540\text{--}670^\circ\text{C}$; Fig. 8a).

Conceptually, the wide range of $P\text{--}T$ conditions determined for ‘peak’ metamorphism via the Ti-in-biotite thermometer and pseudo-section analysis are difficult to reconcile with age data suggesting that samples in both localities formed soon after San Isabel granite intrusion.

Due to dense forestation hindering field investigation and the unknown 3-D structure of the granite pluton itself, it is unclear whether the Marion Mine and Amethyst Prospect localities exist at considerably different distances from the granite–country rock interface. If so, thermal gradients imparted onto the country rock as a result of magma intrusion imply that rocks in each locality experienced different peak temperatures during contact metamorphism. The $P\text{--}T$ conditions of San Isabel granite intrusion have been investigated by Cullers et al. (1992), who used a combination of the Al-in-hornblende barometer and two-feldspar thermometry to constrain crystallization at $\sim 4.5\text{--}7.5$ kbar and a minimum temperature of $\sim 800 \pm 25^\circ\text{C}$ (Fig. 8b). These conditions correlate well with a common field of overlap interpreted for peak metamorphism in samples 17SIMM01, 17SIMM02, and 17SIAP02, as determined by petrological modeling (cf. Fig. 7).

6. Discussion and conclusions

6.1. Tectonic implications for evolution of the Wet Mountains

Previous study of the Wet Mountains shows that the entire region represents a tilted section through the Mesoproterozoic continental crust. Relatively shallow lithologies exposed in the northwest preserve peak $P\text{--}T$ conditions of ~ 3.5 kbar and $\sim 600^\circ\text{C}$ (Goodge and Siddoway, 1997; Siddoway et al., 2000), and relatively deeper lithologies exposed in the southeast show regional metamorphic assemblages with peak $P\text{--}T$ conditions of $\sim 5\text{--}6$ kbar and $\sim 700\text{--}720^\circ\text{C}$ (Levine et al., 2013). While petrological study has been made of rocks from the far southeast corner in close proximity to the San Isabel granite intrusion, no prior thermobarometry or geochronology has been performed, leading to uncertainty about the tectonothermal significance of the unusual mineral parageneses documented above.

In-situ U-Pb dating of monazite in sapphirine hornfels and migmatitic garnet–biotite gneiss constrains the age of metamorphism in both Marion Mine and Amethyst Prospect localities to c. 1340–1320 Ma (Fig. 6), closely post-dating emplacement of the San Isabel granite (1362 \pm 7 Ma; Bickford et al., 1989). Notably, these metamorphic ages are c.

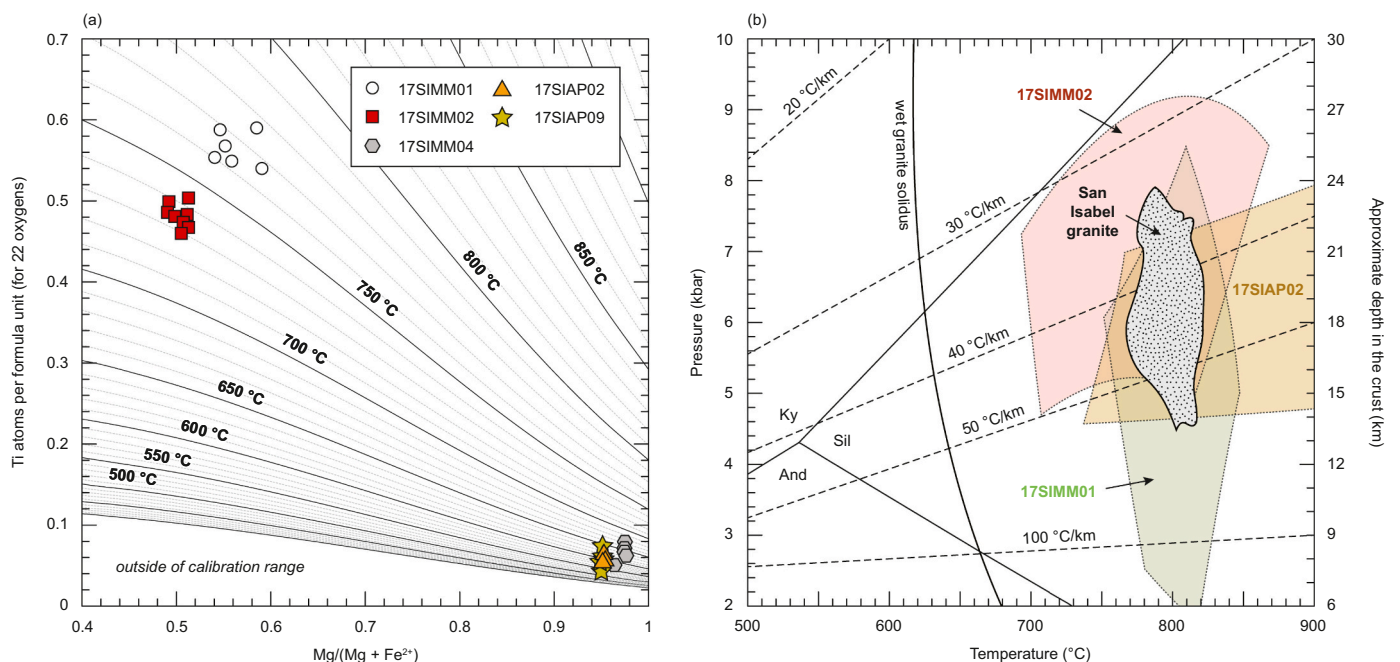


Fig. 8. Results of additional thermobarometry performed on samples from the Wet mountains. (a) Compositions of biotite plotted on the X_{Mg} vs Ti cpfu (for 22 oxygens) diagram of Henry et al. (2005). (b) $P\text{--}T$ grid showing the aggregated results of pseudosection modeling compared to the estimated $P\text{--}T$ conditions of crystallization in the San Isabel granite, shown as a stippled region (from Cullers et al., 1992). Shaded regions mark the interpreted peak $P\text{--}T$ conditions for samples 17SIMM01, 17SIMM02, and 17SIAP02. And – andalusite; Ky – kyanite; Sil – sillimanite.

100 Myr younger than those for amphibolites exposed near Rattlesnake Gulch in the central Wet Mountains (Fig. 2a), which are the nearest dated metamorphic units. Given this gap in time between the ages of peak metamorphism, but close correlation with San Isabel granite emplacement, the samples documented herein are interpreted to have formed during contact metamorphism, as opposed to preserving pre-intrusion regional metamorphic conditions.

Two-feldspar thermometry and Al-in-hornblende barometry performed on the San Isabel granite by Cullers et al. (1992) suggested P - T conditions of crystallization of ~ 4.5 – 7.5 kbar and $\sim 800 \pm 25$ °C (Fig. 8b), equivalent to depths within the Mesoproterozoic crust of ~ 15 – 24 km. The upper limits of this range are likely most appropriate for this intrusion, given the documented northwest-to-southeast increase in metamorphic grade within the Wet Mountains and ~ 5 – 6 kbar calculated pressure of equilibration in Rattlesnake Gulch amphibolites (Levine et al., 2013). Given that these P - T constraints were obtained from magmatic amphibole thermometry and barometry (Cullers et al., 1992), we interpret them to represent the middle to end-stages of crystallization, indicating that the magmatic temperature during intrusion could have been slightly higher. Additionally, while A-type granites are classically considered to have low volatile contents, especially if derived from partial melting of mafic source rocks, the San Isabel granite may be an exception to this rule, as many petrological features in the studied rocks document the importance of fluid–rock interaction during contact metamorphism.

Firstly, aside from marble 17SIAP04, all studied metasedimentary and meta-igneous samples contain large volume proportions of halogen-bearing phases, with F being notably more abundant than Cl (Tables 2 and 3). While the paucity of Cl does not imply that the granite or its expelled fluids were Cl-poor; simply that Cl, if present, was not incorporated into the newly recrystallized phases in the contact aureole. Unfortunately, there are no published chemical analyses of the halogen contents of the San Isabel granite or adjacent plutons to confirm that these bodies represent the sources of halogen rich fluids, which represents a crucial area for future research in this region. Regardless, phlogopite in sapphirine hornfels and calc-silicate samples typically contains up to ~ 3.2 wt% F, clinoamphibole consistently contains between ~ 0.2 wt% F (17SIMM01) and ~ 1.2 wt% F (17SIAP09), and clinohumite in 17SIMM04 contains ~ 2 wt%. The source of these halogens is interpreted to be the San Isabel granite itself, as F has an average concentration in the Earth's crust of just ~ 625 ppm (Taylor, 1964), meaning that the lithologies documented here are strongly enriched. Primitive mafic igneous rocks, such as IAT basalts, have an average F content of 130 ppm, although submarine hydrothermal activity can elevate this to ~ 400 ppm (Koga and Rose-Koga, 2018). Clastic sedimentary rocks themselves may vary according to the mineralogy of their constituent grains, although typically have F contents < 1000 ppm (Koga and Rose-Koga, 2018). However, SiO_2 -saturated intermediate and felsic magmas may contain up to 15,000 ppm, and so represent significant reservoirs and sources of halogens within the lithosphere.

Secondly, microstructural evidence for the influence of thermal metamorphism and fluid-mediated recrystallization is evidenced by the lack of foliation within mica- and amphibole-rich units (Fig. 4b and d). Mechanical stresses imparted on country rocks due to magma emplacement are considered negligible, regardless of the size of the intrusion, although the prevalence of ductilely deformed orthogneiss, paragneiss, and amphibolite exposed in Williams Creek just 5 km south of the study area (Fig. 2a) supports the interpretation that coarse and randomly oriented phlogopite and tschermakite hornfelsic textures record static recrystallization and annealing at high temperatures. The lack of deviatoric stress applied to these units during recrystallization may also account for the interpreted formation and in-situ recrystallization of small volumes of partial melt in sample 17SIMM01. While melt volumes may ascend and flow out of their local environment of formation due to buoyancy once a critical threshold is reached (Palin et al., 2016b), this process is greatly facilitated by the presence of strong

petrological anisotropy (e.g. foliations), and thus may be impeded during short-term residence at suprasolidus conditions by hornfelsic or granofelsic rock fabrics.

Rocks of the Colorado Front Range, including those within the Wet Mountains, preserve widespread structural and metamorphic evidence for multiple major episodes of crustal deformation associated with terrane accretion and the growth of Laurentia (Whitmeyer and Karlstrom, 2007). The oldest geological activity in the Wet Mountains is documented by c. 1705 Ma magmatism in the northernmost exposures (Fig. 2a) and northeast–southwest trending deformation associated with the Yavapai collisional orogeny (Bickford et al., 1989; Daniel et al., 2013). Slightly younger c. 1606 Ma granodiorite plutons and overprinting fabrics preserve evidence for subsequent accretion of the Mazatzal Province to the south (Bickford et al., 1989; Siddoway et al., 2000). Both of these events record collisional orogenesis, although the bulk of exposed lithologies in the central and southern sections of the Wet Mountains formed even later, after an apparent tectonic lull of c. 150–200 Myr. Widespread emplacement of A-type granitoids throughout the west–central U.S.A. between c. 1460 Ma and c. 1350 Ma provides evidence for a period of extended crustal heating apparently unrelated to terrane accretion, termed the Picuris orogeny (Shaw and Karlstrom, 1999; Sims and Stein, 2003). The cause of this metamorphic–magmatic event is currently unresolved, although metamorphic ages of c. 1340–1320 Ma in our samples support its occurrence in southern Colorado.

While some workers support the petrogenesis of A-type granitoids in extensional geodynamic regimes (e.g. Zhou et al., 2006), such a scenario does not correlate with currently understood plate-tectonic models for the growth of Laurentia (Hoffman, 1991; Whitmeyer and Karlstrom, 2007), which experienced numerous accretionary events via collisional orogeny. Further, if lithospheric thinning were responsible for San Isabel granite formation, the geothermal gradients of contact metamorphism in the adjacent crust would likely be much higher than calculated here (~ 40 – 50 °C/km; Fig. 8b) and more pervasively documented throughout the Wet Mountains, as mantle up-welling through lithospheric extension or the introduction of deeply sourced, dry mafic magmas, which are effective geological mechanisms for increasing heat flow within the lower and middle crust (Huang et al., 2021). Although the rocks studied here are slightly younger than those representing exposed middle crust in the central and southern Wet Mountains due to overprinting contact metamorphism, the lack of tectonic discontinuities between them implies that all experienced the same pre-magmatic tectonothermal evolution. As such, we interpret that these c. 1.46–1.35 Ga-related magmatic and metamorphic events are associated with crustal thickening and compression, as shown by strongly deformed schists elsewhere throughout the Wet Mountains. The absence of a strong foliation in the studied units can be ascribed to metamorphic recrystallization during contact metamorphism, which induced pervasive changes to their mineralogy and fabrics. Further study throughout the west–central U.S.A. is required to constrain the driving forces responsible given the current absence of a discrete 'Picuris' continental terrane.

6.2. Protolith and bulk-composition control on the development of unusual mineral assemblages

The metamorphic facies concept states that P , T , and bulk-rock composition all fundamentally control the mineral assemblages that stabilize in a rock during burial and heating. The P - T conditions of metamorphism identified here (~ 6 kbar and ~ 800 °C; Fig. 8b) are not unusual for contact metamorphism in the middle continental crust, therefore the unusual mineral assemblages in sapphirine hornfels from Amethyst Prospect must have formed due to unusual bulk-rock composition characteristics. Whole-rock geochemistry indicates that samples 17SIAP02 and 17SIAP09 are strongly aluminous (~ 34 wt% Al_2O_3) and magnesian (~ 17 wt% MgO) compared to all other samples collected from the field area (Table 1). Such hyper-aluminous bulk-rock

compositions are unlike any common clastic sedimentary and volcanic protoliths expected to occur in collisional orogens, such as shale (17.5 wt%: [Ague, 1991](#)), graywacke (15.5 wt%: [Floyd et al., 1991](#)), andesite (17.2 wt%: [Middlemost, 1985](#)), and rhyolite (13.3 wt%: [Nockolds, 1954](#)). Two end-member scenarios can thus be considered for their petrogenesis: either these lithologies acted as closed chemical systems during metamorphism, such that the protolith did have these unusual geochemical characteristics, or substantial open-system mass-transfer occurred during metamorphism, allowing localized enrichment in Al_2O_3 and MgO compared to adjacent lithologies.

If the sapphirine hornfels' protoliths acted as closed chemical systems during metamorphism, Al-enrichment must have occurred during their pre-metamorphic history, thus "priming" the samples to have bulk compositions conducive to sapphirine and corundum growth at amphibolite-facies P - T conditions. Potential protoliths in this case include bauxitic sediments or laterites, which form in tropical climates where surface weathering and leaching of mobile components is intense. While a possibility, the paleolatitude of the Yavapai Province at c. 1.8 Ga, immediately prior to the onset of accretion to the southeastern margin of Laurentia, is poorly constrained ([Murphy et al., 2004](#)), rendering this solution inconclusive. In addition, laterite formation is spatially extensive, yet the hyper-aluminous metasediments documented here have only been reported from localized outcrops immediately adjacent to the San Isabel granite, although this does not exclude the possibility of their widespread occurrence in the subsurface. Alternatively, Al_2O_3 may have been concentrated in the metamorphic environment by percolating fluids removing more soluble components, such as alkalis, and leaving behind relatively immobile species ([Ague, 1991](#)). Such fluid-rock interaction is considered very likely in this case, given the high volatile content of these samples (Table 1: ~3.6–3.8 wt%) and microstructural evidence for phlogopite stability at peak metamorphism (Fig. 4b). Additional support for fluid-mediated metasomatism, as discussed above, is the high F content of the mica and amphibole in almost all studied samples (Tables 2–3), as felsic granitoids intrusions represent major sources of halogens ([Koga and Rose-Koga, 2018](#)) that can be liberated into the adjacent country rock upon solidification.

Minor- and trace-element signatures in sapphirine hornfels samples 17SIAP02 and 17SIAP09 further preclude some common rock types as being potential precursors, assuming that the components considered are relatively immobile and preserve their parental ratios during high-grade metamorphism. Low Cr and Ni contents (Table S1) preclude an ultramafic or mafic precursor, and low U, V, and Sr (Table S1) argues against these units being metamorphosed evaporite salts. However, pervasive Zn and Cu mineralization in samples collected from both prospects, as shown by the abundance of galena and zincian spinel in 17SIMM04, supports the interpretation that some rocks within this tectonostratigraphic sequence have a seafloor origin. Metamorphic spinel (*sensu lato*) commonly forms in hydrothermally altered metasedimentary and metavolcanic rocks, aluminous granulites, granitic pegmatites, and banded iron formations, although it has distinctly different Zn–Fe–Mg ratios in each ([Heimann et al., 2005](#)). Fig. 9 shows a protolith discrimination diagram for the gahnite–hercynite–spinel ternary system, on which compositional data from samples 17SIMM04, 17SIAP02, 17SIAP04, and 17SIAP09 are shown. While spinel and pleonast from sapphirine hornfels samples contain very little Zn.

(Table 3), forsterite-bearing calc-silicate 17SIMM04 contains gahnitic spinel with ~14 wt% ZnO (Table 2), which falls within the fields delimited by marbles and metamorphosed volcanogenic massive sulfide (VMS) deposits associated with Mg–Ca–Al alteration zones. As such, these units likely formed in a deep marine geological setting associated with pervasive hydrothermal activity, such as occurs near to mid-oceanic ridge spreading centers today ([Herna'ndez-Urbe et al., 2020](#)).

The wide-ranging provenances of rocks exposed within the San Isabel granite aureole is potentially confusing at first glance, but can be reconciled with the known geological history of the Colorado Front Range, as the Yavapai and Mazatzal orogenies record sequential

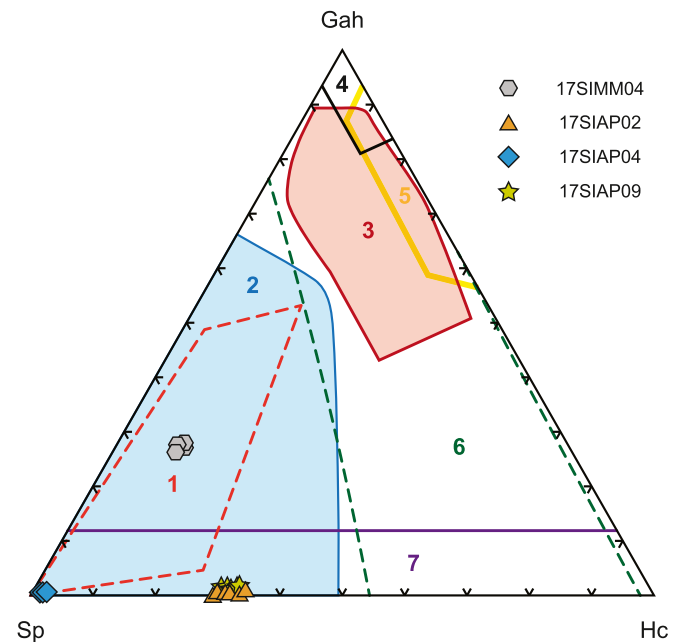


Fig. 9. Protolith discrimination diagram for spinel compositions in terms of gahnite (Gah), hercynite (Hc), and spinel (Sp) end-members reported from (1) marbles, (2) metamorphosed massive sulfide deposits associated with Mg–Ca–Al alteration zones, (3) metamorphosed massive sulfide deposits associated with Fe–Al metasedimentary and metavolcanic rocks, (4) metabauxites, (5) granitic pegmatites, (6) unaltered and hydrothermally altered Fe–Al-rich metasedimentary and metavolcanic rocks, and (7) Al-rich granulites (Gah < 12 mol %) (after [Heimann et al., 2005](#)). Spinel compositions from samples 17SIMM04, 17SIAP02, 17SIAP04, and 17SIAP09 are shown.

microcontinent accretion to the southern margin of the Archean Wyoming Craton ([Whitmeyer and Karlstrom, 2007](#)). Amphibolite collected from the Marion Mine has an IAT trace element signature, so likely formed in an intra-oceanic arc environment between the Yavapai and Mazatzal Provinces, whereas shallow-marine carbonates and calc-silicates may have stabilized on an adjacent continental shelf. The close association of metamorphosed VMS deposits or pelagic sediments showing evidence for localized hydrothermal activity indicates that this entire lithostratigraphic sequence observed in the southern Wet Mountains may have originally accumulated in a forearc basin, with all rock types having been obducted or otherwise incorporated between two colliding continental fragments during Mesoproterozoic plate convergence.

6.3. Stabilization of nominally high-temperature minerals at low-grade conditions

While the samples documented here only experienced upper amphibolite-facies peak metamorphism, they contain minerals that are typically found at higher-grade conditions. Much discussion in this work has focused on sapphirine, which has become synonymous in recent years with UHT metamorphism of Al-rich metasedimentary rocks, although this is only diagnostic when coexisting with quartz ([Kelsey and Hand, 2015](#)). Sapphirine has two naturally occurring end-members that preferentially stabilize in different P - T regimes. Detailed crystallographic analysis via X-ray diffraction ([Fleet, 1967](#)) suggests compositions that range between an Mg- and Si-rich form ($\text{Mg}_2\text{Al}_4\text{Si}_2\text{O}_{10}$)₄ and an Al-rich form ($\text{Mg}_7\text{Al}_{18}\text{Si}_3\text{O}_{40}$), related by the Tschermak's substitution $\text{Mg} + \text{Si} = 2\text{Al}$. These end-members are referred to as 2:2:1 and 7:9:3, respectively. Deviation from this ideal binary solid solution occurs via incorporation of minor amounts of (Mg, Fe, Mn, Ni)O, (Al, Fe, Cr, V, Ti)₂O₃, or – rarely – beryllium ([Goscombe, 1992](#)). A Si-poor and even more Al-rich analogue of sapphirine has been synthesized in

experiments, but has not been documented in nature, and has the theoretical end-member composition $\text{Mg}_6\text{Al}_{20}\text{Si}_2\text{O}_{40}$ (or 3:5:1: Grew et al., 2008).

Fig. 10a shows a compilation of metamorphic sapphirine compositions reported in the literature, binned by temperature of formation (Table S3). These natural data show a clear compositional progression with temperature, with low-grade examples plotting between the 3:5:1 and 7:9:3 forms, whereas high-grade grains have compositions that trend towards the 2:2:1 form. True UHT sapphirines ($>900^\circ\text{C}$) are thus commonly Al-poor and Si-rich (Fig. 10a). Analyses from Wet Mountains samples (Table 3) correlate within compositional clusters from the literature that equilibrated at non-UHT ($<900^\circ\text{C}$) conditions (Fig. 10b) and lie off the ideal mixing line owing to substitution of minor components, including $\sim 2.7\text{ wt}\%$ Fe_2O_3 (Table 3). Indeed, experimental data and the results of petrological modeling show that incorporation of Fe^{3+} into the sapphirine structure expands its stability to low temperatures. This compositional correlation with natural examples further supports interpretations made from thermobarometry (Fig. 7c) that the sapphirine-bearing hornfels documented from Amethyst Prospect formed at upper-amphibolite facies conditions during contact metamorphism, thus adding these lithologies to a small (but growing) set of lithologies where sapphirine is known to be stable at low-grade P - T conditions.

While the bulk compositions, mineral assemblages, and interpreted thermal conditions of equilibration documented here for 17SIAP02 and 17SIAP09 are unusual, they are not unique. Nijland et al. (1998) reported isolated pods of orthopyroxene-, spinel-, and sapphirine-bearing metasediments from the granulite-facies Bamble sector, Norway, which were suggested to have formed at very low-temperature conditions of $\sim 500^\circ\text{C}$ based on Al-in-orthopyroxene thermometry. The occurrence of highly saline fluid inclusions in quartz from these lithologies was used as evidence for in-situ metasomatic alteration of orthogneiss via large-volume fluxing of a low- $a_{\text{H}_2\text{O}}$ aqueous fluid, which promoted localized breakdown of hydrous minerals and stabilization of nominally high-grade anhydrous minerals instead.

Silica-undersaturated phlogopite- and sapphirine-schists more closely resembling those from the Wet Mountains have been reported

from the Arunta Inlier, Australia, by Scrimgeour and Raith (2002). These samples are volumetrically dominated by phlogopite ($>50\text{ vol}\%$) and contain additional cordierite, corundum, and zincian spinel (0.9–3.6 wt % ZnO). Peak P - T conditions of 3 kbar and 650 – 700°C were inferred based on experimentally constrained phase equilibria in the MgO - Al_2O_3 - SiO_2 - H_2O system, also making these samples of contact metamorphic origin. However, in contrast to the results of this study, Scrimgeour and Raith (2002) interpreted the precursor lithology to be an unusually magnesian, aluminous, and potassic evaporitic mudstone, with metasomatism involving saline or halogen-rich fluids during magma crystallization not considered likely.

Finally, Raith et al. (2008) document corundum-, spinel- and sapphirine-bearing anorthitic to phlogopitic rocks that occur in close association with diverse calc-silicate rocks, marbles, and biotite-sillimanite-cordierite gneisses, and show remarkable similarity to the sapphirine hornfels documented in this work. Raith et al. (2008) reported that formation of these “sakenites” occurred via two distinct metasomatic episodes, the first of which was subaerial leaching of kaolinite-rich sediments or calcareous bauxites, which were buried to form anorthite-corundum biminerale assemblages at P - T conditions of ~ 6 – 7 kbar and 800°C . A subsequent influx of Mg-, Si- and K-bearing fluids into these anorthite-corundum rocks at P - T conditions of 6 kbar and 750 – 700°C was interpreted to cause in-situ growth of corundum, spinel, sapphirine, and phlogopite. Interestingly, this two-stage evolution led to the formation of spinel coronae around relic corundum porphyroblasts, although similar microstructures observed in sample 17SIAP02 (Fig. 4a) are suggested here to be of prograde origin.

While each of these examples shows numerous similarities and differences to samples 17SIAP02 and 17SIAP09, one common factor is the influence of aqueous fluid in either “priming” the precursor lithology before heating and burial, or else causing metasomatic alteration within the crustal environment. Fluid-rock interaction in the metamorphic environment has been well studied in the field and laboratory, and using both experimental and numerical modeling. Fluid-driven mass transfer and subsequent mineralogical changes are defining features of metasomatism in silicate rocks, although it can be unclear where metamorphism ends and metasomatism begins. Diagnostic evidence for

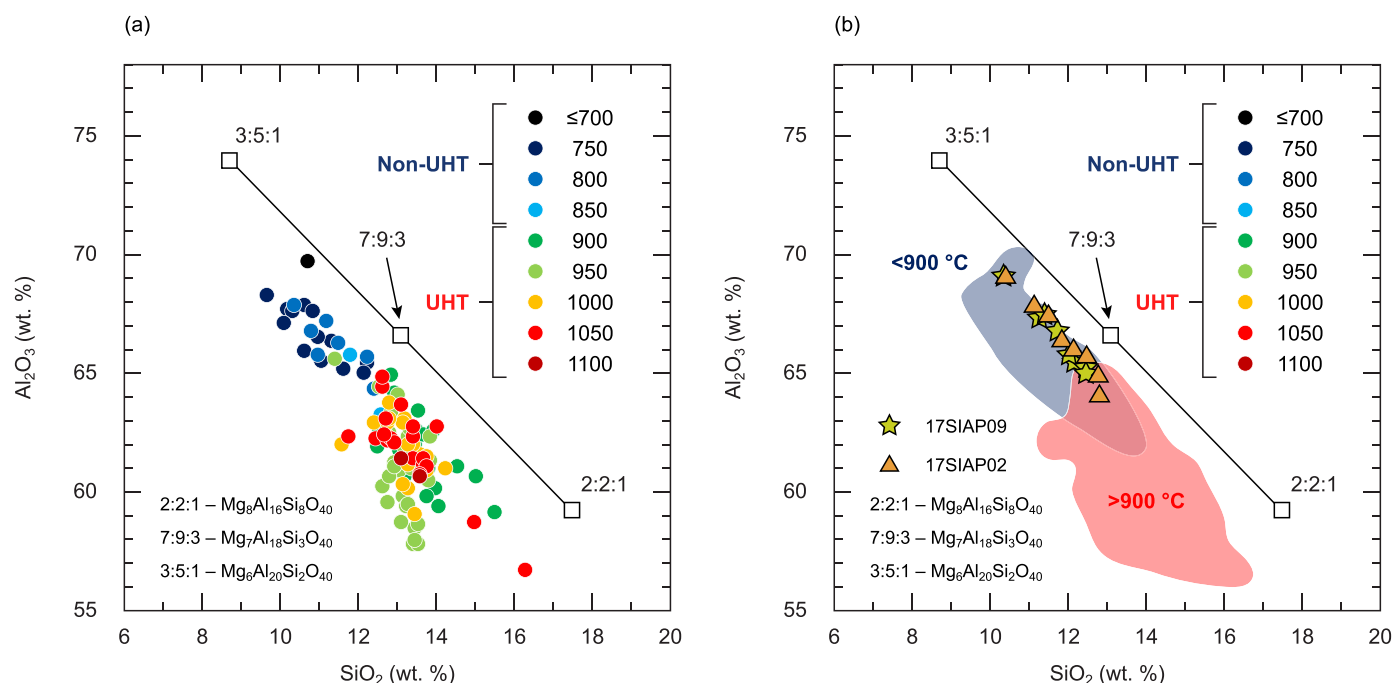


Fig. 10. (a) Compilation of sapphirine compositions reported in the literature, binned by metamorphic temperature of formation ($^\circ\text{C}$). See Table S3 for sources of data. (b) Analyzed compositions from samples 17SIAP02 and 17SIAP09 are shown alongside generalized fields for sub- 900°C (non-UHT) and $>900^\circ\text{C}$ (UHT) sapphirine grains.

massive fluid flow and near-total mineralogical alteration of a precursor rock includes skarns, greisens, and serpentinization of oceanic crust, although without knowledge of the precursor lithology to samples 17SIAP02 and 17SIAP09, quantification of the extent of mineralogical change cannot be performed. Nonetheless, these lithologies may represent intermediate case studies between nominally fluid-poor high-grade metamorphic environments, such as granulite terranes (Warren, 1983), and nominally fluid-rich environments, such as a mantle wedge overlying a devolatilizing subduction slab (Chin and Palin, 2022). Future investigation of similar rocks may help to reveal a complete spectrum of metasomatic processes between these end-members that operate in different geological environments.

6.4. Drawing the line in thermobarometry

The samples documented in this work from the Wet Mountains are petrologically unusual and the application of common thermobarometric techniques has been shown to be fraught with difficulties. Indeed, the data and results presented above raise important philosophical questions about the interpretation and reliability of P - T estimation – simply phrased, how good is ‘good enough’? It is well-known that modeling (*sensu lato*) can never perfectly replicate the geological processes and conditions observed in nature, with discrepancies between the results of calculations and observations made on real rocks accepted as being unavoidable. Numerous studies have quantified errors associated with petrological modeling – specifically the construction and interpretation of pseudosections – that arise due to uncertainties (1) on the physical properties of end-members in thermodynamic datasets and (2) associated with the formulation of a - x relations describing the thermodynamic properties of solid solution mixing of end-members within a single phase. Much experimental end-member mineral data used within thermodynamic datasets was obtained decades ago, and improvements can certainly be made by reproducing such experiments with more advanced equipment that offers a greater control on experimental run conditions. Further sources of error may be analytical in nature, relating to the imprecision of measurement of mineral compositions against which model results are compared, or geological, induced by scale-independent heterogeneity in a rock complicating definition of the extent of an equilibration volume/effective bulk composition. When combined, these multiple sources of error lead to both systematic and random uncertainties in calculated phase equilibria that render the results reliable only at a fairly coarse scale, and the user of such techniques should never blindly accept the model outputs. After all, the rocks under study are naturally ‘right’, and the blame for discrepancies that emerge between what is observed and what is modeled must always fall on the side of the calculations – not nature.

Four rocks were subject to pseudosection analysis in this work, with model results in each showing varying degrees of discrepancy with petrographic observations. Marble sample 17SIAP04 showed the closest match between observed and calculated mineral proportions, although this is unsurprising given the simple compositional system considered (CFMASHOC) and nearly pure Mg end-member compositions for spinel and forsterite (Table 3). While calculated vs. observed mineral proportions showed some level of disagreement, there is notable uncertainty in estimations of 3-D volumes when examining 2-D sections of anisotropic systems. As such, volume discrepancies on the order of 2–3% should be considered acceptable by most workers who deal with this phase diagram-based technique.

Migmatitic garnet–biotite gneiss sample 17SIMM02 showed the next-best level of agreement between calculated and observed phase assemblages. Here, volumes matched well, although additional magnetite (< 1 vol%) was calculated to be present, but was not observed in the sample. In the authors’ opinions, such a discrepancy should also be considered insignificant, and the presence of minor and accessory phases in interpreted peak assemblage fields can be accounted for as a function of imperfect a - x models, bulk-composition uncertainty, or

localized metastability.

Calculated phase equilibria for amphibolite sample 17SIMM01 did not allow for direct constraints to be placed on the conditions of metamorphism, owing to the predicted stabilization of augite and partial melt at P - T conditions matching those obtained from Ti-in-biotite thermometry (Fig. 8a) and pseudosection analysis of 17SIMM02 and 17SIAP04 (Fig. 7b–c). The overstabilization of augite in the latest generation of a - x models (Green et al., 2016) has been recognized by numerous workers (Forshaw et al., 2019; Santos et al., 2019) and quantified here in the subsolidus regime to be significant. Calculated phase equilibria for 17SIMM01 predict up to 5 vol% augite at the point of first melting, which appears to be a common issue found in models of many types of meta-mafic rocks using these a - x relations, but does not agree with the results of most experiments. In the suprasolidus regime, augite volume is predicted to rise owing to the breakdown of amphibole and quartz, which also produces partial melt (Palin et al., 2016c); however, despite careful petrographic examination, no evidence for partial melting was observed in 17SIMM01 at either the thin section or hand sample scale. Thus, by contrast with samples 17SIMM02 and 17SIAP04, the discrepancies between observed and calculated phase equilibria for this amphibolite appear too large to be explained by the influence of additional components not considered in the chemical system (e.g. F in amphibole: Table 2). Sapphirine hornfels sample 17SIAP02 revealed similar issues, whereby voluminous orthopyroxene (~15 vol%) was predicted to be stable in an assemblage field that otherwise matches the observed mineralogy well and correlates with independently estimated P - T conditions. Akin to sample 17SIMM01, the occurrence of abundant halogens in mica in sample 17SIAP02 (Table 3) necessarily adds complexity to the calculated phase equilibria, although no parameterizations for high-temperature halogen-bearing mica or amphibole a - x relations currently exist to allow quantification of the effects of such substitutions. Additional experimental data constraining the behavior and partitioning of minor elements such as F between silicate phases at these P - T conditions should allow such problems to be addressed more coherently.

Are solutions available to solve these petrological problems? From a near-term perspective, the answer is no. Shortcomings in the actual or perceived ability of conventional thermobarometers to constrain P - T conditions of metamorphism in parageneses that differ from those used for calibration cannot be directly circumvented. In particular, most empirical thermobarometers were calibrated without evaluation of substitutions of minor elements, such as Fe³⁺ in biotite, and their application necessarily assumes full chemical equilibration between constituent phases. Whether or not this is a suitable assumption for crustal metamorphism is a topic of much current debate, especially during short-duration tectonothermal events, such as contact metamorphism.

Consequently, many workers now favor the use of phase diagram-based techniques that are typically not constrained by the minerals that exist in an assemblage, as long as thermodynamic data exist for their end-members. Indeed, pseudosections have even been applied to quantify the petrological effects of disequilibrium, thus potentially allowing new ways to account for discrepancies between observed and calculated phase equilibria. These possibilities provide exciting new avenues for study that may help to reshape our understanding of petrological processes on Earth, both in young tectonic terranes and in the deep geological past.

Supplementary data to this article can be found online at <https://doi.org/10.1016/j.lithos.2023.107024>.

Declaration of Competing Interest

The authors declare the following financial interests/personal relationships which may be considered as potential competing interests:

Zachary Palmer reports financial support was provided by Geological Society of America. Juan David Hernandez Montenegro reports financial

support was provided by Research Division (DIB) of the Universidad Nacional de Colombia.

Acknowledgements

This work was conducted whilst RMP, ZP, and DHU were based at the Colorado School of Mines (CSM), and was part-funded by awards and research grants provided by the Geological Society of America and the Rocky Mountain Association of Geologists. RMP acknowledges startup funds provided by CSM for supporting fieldwork and associated analytical costs. JDHM visited CSM thanks to funding provided by the Research Division (DIB) of the Universidad Nacional de Colombia. Katharina Pfaff, Yvette Kuiper, and Ric Wendlandt are thanked for discussion. Dave Waters and Jay Ague are thanked for comments on an earlier version of the work, and Daniel Harlov and an anonymous reviewer are thanked for their comments on the final version of this work, all of which strengthened the manuscript considerably. Finally, Nadia Malaspina is thanked for her efficient editorial handling.

References

- Ague, J.J., 1991. Evidence for major mass transfer and volume strain during regional metamorphism of pelites. *Geology* 19, 855–858.
- Aleinikoff, J.N., Walter, M., Lyttle, P.T., Burton, W.C., Leo, G.W., Nelson, A.E., Schindler, J.S., Southworth, C.S., 1993. U–Pb Zircon and Monazite Ages of Middle Proterozoic Rocks, Northern Blue Ridge, Virginia. *GSA Abstract*, 25.
- Aleinikoff, J.N., Schenck, W.S., Plank, M.O., Srogi, L., Fanning, C.M., Kamo, S.L., Bosbyshell, H., 2006. Deciphering igneous and metamorphic events in high-grade rocks of the Wilmington complex, Delaware: morphology, cathodoluminescence and backscattered electron zoning, and SHRIMP U–Pb geochronology of zircon and monazite. *Geol. Soc. Am. Bull.* 118, 39–64.
- Amato, J.M., Boullion, A.O., Serna, A.M., Sanders, A.E., Farmer, G.L., Gehrels, G.E., Wooden, J.L., 2008. Evolution of the Mazatzal province and the timing of the Mazatzal orogeny: insights from U–Pb geochronology and geochemistry of igneous and metasedimentary rocks in southern New Mexico. *Geol. Soc. Am. Bull.* 120, 328–346.
- Anderson, J.L., Cullers, R.L., 1999. Paleo- and Mesoproterozoic granite plutonism of Colorado and Wyoming. *Rocky Mt. Geol.* 34, 149–164.
- Aranoich, L.Y., Newton, R., Manning, C., 2013. Brine-assisted anatexis: experimental melting in the system haplogranite–H₂O–NaCl–KCl at deep-crustal conditions. *Earth Planet. Sci. Lett.* 374, 111–120.
- Aronoff, R.F., Andronikos, C.L., Vervoort, J.D., Hunter, R.A., 2016. Redefining the metamorphic history of the oldest rocks in the southern Rocky Mountains. *Geol. Soc. Am. Bull.* 128, 1207–1277.
- Bennett, V.C., DePaolo, D.J., 1987. Proterozoic crustal history of the western United States as determined by neodymium isotopic mapping. *Geol. Soc. Am. Bull.* 99, 674–685.
- Bickford, M.E., Cullers, R.L., Shuster, R.D., Premo, W.R., Van Schmus, W.R., 1989. U–Pb zircon geochronology of Proterozoic and Cambrian plutons in the Wet Mountains and southern front range, Colorado. In: Grambling, J.A., Tewksbury, B.J. (Eds.), *Proterozoic Geology of the Southern Rocky Mountains*. Vol. 235. Geological Society of America, pp. 49–64.
- Bosi, F., Biagioni, C., Pasero, M., 2018. Nomenclature and classification of the spinel supergroup. *Eur. J. Mineral.* 31, 183–192.
- Chin, E.J., Palin, R.M., 2022. Water storage in cratonic mantle. *Terra Nova* 34 (5), 369–380.
- Coleman, D.S., Bath, A.P., Wooden, J.L., 2002. Early to middle Proterozoic construction of the Mojave province, southwestern United States. *Gondwana Res.* 5, 75–78.
- Cullers, R.L., Griffin, T., Bickford, M.E., Anderson, J.L., 1992. Origin and chemical evolution of the 1360 Ma San Isabel batholith, Wet Mountains, Colorado: a mid-crustal granite of anorogenic affinities. *Geol. Soc. Am. Bull.* 104, 316–328.
- Daniel, C.G., Pfeifer, L.S., Jones III, J.V., McFarlane, C.M., 2013. Detrital zircon evidence for non-Laurentian provenance, Mesoproterozoic (ca. 1490–1450 Ma) deposition and orogenesis in a reconstructed orogenic belt, northern New Mexico, USA: defining the Picuris orogeny. *Geol. Soc. Am. Bull.* 125, 1423–1441.
- Diener, J.F.A., Powell, R., White, R.W., Holland, T.J.B., 2007. A new thermodynamic model for clino- and orthoamphiboles in the system Na₂O–CaO–FeO–MgO–Al₂O₃–SiO₂–H₂O–O. *J. Metamorph. Geol.* 25, 631–656.
- Ellis, D.J., Thompson, A.B., 1986. Subsolidus and partial melting reactions in the quartz-excess CaO–MgO–Al₂O₃–SiO₂–H₂O system under water-excess and water-deficient conditions to 10 kbar: some implications for the origins of peraluminous melts from mafic rocks. *J. Petrol.* 27, 91–121.
- Eskola, P., 1914. On the petrology of the Orijärvi region in southwestern Finland. *Bulletin de la Commission géologique de Finlande* 40, 277.
- Fleet, S.G., 1967. Non-space-group absences in sapphirine. *Mineral. Mag.* 36, 449–450.
- Floyd, P.A., Shail, R., Leveridge, B.E., Franke, W., 1991. Geochemistry and provenance of Rhenohercynian synorogenic sandstones: implications for tectonic environment discrimination. *Geol. Soc. Lond. Spec. Publ.* 57, 173–188.
- Forshaw, J.B., Waters, D.J., Pattison, D.R.M., Palin, R.M., Goopon, P., 2019. A comparison of observed and thermodynamically predicted phase equilibria and mineral compositions in mafic granulites. *J. Metamorph. Geol.* 37, 153–179.
- Frost, B.R., Chacko, T., 1989. The granulite uncertainty principle: limitations on thermobarometry in granulites. *J. Geol.* 97, 435–450.
- Frost, C.D., Frost, B.R., Chamberlain, K.R., Hulsebosch, T.P., 1998. The late Archean history of the Wyoming province as recorded by granitic magmatism in the Wind River Range, Wyoming. *Precambrian Res.* 89, 145–173.
- Goodge, J.W., Siddoway, C.S., 1997. Mineral reactions and petrogenetic implications of Fe–Mn-andalusite, northern Wet Mountains, Colorado. *Geol. Soc. Am. Abstr. Programs* 29, 11.
- Goscombe, B.D., 1992. Silica-undersaturated sapphirine, spinel and kornerupine granulite facies rocks, NE Strangways Range, Central Australia. *J. Metamorph. Geol.* 10, 181–201.
- Green, E.C.R., White, R.W., Diener, J.F.A., Powell, R., Holland, T.J.B., Palin, R.M., 2016. Activity–composition relations for the calculation of partial melting equilibria for metabasic rocks. *J. Metamorph. Geol.* 34, 845–869.
- Grew, E.S., Halenius, U., Pasero, M., Barbier, J., 2008. Recommended nomenclature for the sapphirine and surinamite groups (sapphirine supergroup). *Mineral. Mag.* 72, 839–876.
- Harley, S.L., 1998. On the occurrence and characterisation of ultrahigh-temperature (UHT) crustal metamorphism. In: Treloar, P.J., O'Brien, P.J. (Eds.), *What Drives Metamorphic Reactions?* Vol. 138. The Geological Society, London, Special Publication, pp. 75–101.
- Heimann, A., Spry, P.G., Teale, G.S., 2005. Zincian spinel associated with metamorphosed Proterozoic base-metal sulfide occurrences, Colorado: a re-evaluation of gahnite composition as a guide in exploration. *Can. Mineral.* 43, 601–622.
- Henry, D.J., Guidotti, C.V., Thompson, J.A., 2005. The Ti-saturation surface for low-to-medium pressure metapelitic biotite: implications for geothermometry and Ti-substitution mechanisms. *Am. Mineral.* 90, 316–328.
- Hernández-Montenegro, J.D., Andronikos, C.L., Zuluaga, C.A., Aronoff, R.F., 2019. Effects of melt loss, melt retention, and protolith composition on differentiation of anatectic metapelites: a case study of the wet mountains, Colorado. *Lithos* 344, 425–439.
- Hernández-Urbe, D., Palin, R.M., Cone, K.A., Cao, W., 2020. Petrological implications of seafloor hydrothermal alteration of subducted mid-ocean ridge basalt. *J. Petrol.* 61 (9) ega086.
- Hoffman, P.F., 1988. United plates of America, the birth of a craton: early Proterozoic assembly and growth of Laurentia. *Annu. Rev. Earth Planet. Sci.* 16, 543–603.
- Hoffman, P.F., 1991. Did the breakout of Laurentia turn Gondwanaland inside out? *Science* 252, 1409–1412.
- Huang, G., Guo, J., Palin, R., 2021. Phase equilibria modeling of anatexis during ultrahigh temperature metamorphism of the crust. *Lithos* 398, 106326.
- Jessup, M.J., Jones III, J.V., Karlstrom, K.E., Williams, M.L., Connelly, J.N., Heizler, M.T., 2006. Three Proterozoic orogenic episodes and an intervening exhumation event in the Black Canyon of the Gunnison region, Colorado. *J. Geol.* 114, 555–576.
- Jones III, J.V., Daniel, C.G., Doe, M.F., 2015. Tectonic and sedimentary linkages between the Belt–Purcell basin and southwestern Laurentia during the Mesoproterozoic, ca. 1.60–1.40 Ga. *Lithosphere* 7, 465–472.
- Jones, D.S., Snoke, A.W., Premo, W.R., Chamberlain, K.R., 2010. New models for Paleoproterozoic orogenesis in the Cheyenne belt region: evidence from the geology and U–Pb geochronology of the big Creek Gneiss, southeastern Wyoming. *Geol. Soc. Am. Bull.* 122, 1877–1898.
- Kelsey, D.E., Hand, M., 2015. On ultrahigh temperature crustal metamorphism: phase equilibria, trace element thermometry, bulk composition, heat sources, timescales and tectonic settings. *Geosci. Front.* 6, 311–356.
- Koga, K.T., Rose-Koga, E.F., 2018. Fluorine in the Earth and the solar system, where does it come from and where can it be found? *C. R. Chim.* 21, 749–756.
- Levine, J.S., Mosher, S., Siddoway, C.S., 2013. Relationship between syn-deformational partial melting and crustal-scale magmatism and tectonism across the Wet Mountains, Central Colorado. *Lithosphere* 5, 456–476.
- Mahan, K.H., Allaz, J.M., Baird, G.B., Kelly, N.M., 2013. Proterozoic metamorphism and deformation in the northern Colorado Front Range. *Geol. Soc. Am.: Field Guides* 33, 185–204.
- Middlemost, E.A.K., 1985. *Magmas and Magmatic Rocks: An Introduction to Igneous Petrology*. Longman, London.
- Murphy, B.J., Pisarevsky, S.A., Nance, D.R., Keppie, D.J., 2004. Neoproterozoic–early paleozoic evolution of peri-Gondwanan terranes: implications for Laurentia–Gondwana connections. *Int. J. Earth Sci.* 93, 659–682.
- Nijland, T.G., Touret, J.L., Visser, D., 1998. Anomalous low temperature orthopyroxene, spinel, and sapphirine occurrences in metasediments from the Bamble amphibolite-to-granulite facies transition zone (South Norway): possible evidence for localized action of saline fluids. *J. Geol.* 106, 575–590.
- Nockolds, S.R., 1954. Average chemical compositions of some igneous rocks. *Geol. Soc. Am. Bull.* 65, 1007–1032.
- Oshetski, K.C., Kucks, R.P., 2000. Colorado aeromagnetic and gravity maps and data; a web site for distribution of data. *U.S. Geol. Surv. Open File Rep.* 42.
- Palin, R.M., Dyck, B., 2021. Metamorphism of pelitic (al-rich) rocks. In: *Encyclopedia of Geology*, second edition. Elsevier, Cambridge, USA, pp. 445–456.
- Palin, R.M., Weller, O.M., Waters, D.J., Dyck, B., 2016a. Quantifying geological uncertainty in metamorphic phase equilibria modelling: a Monte Carlo assessment and implications for tectonic interpretations. *Geosci. Front.* 7, 591–607.
- Palin, R.M., White, R.W., Green, E.C.R., 2016b. Partial melting of metabasic rocks and the generation of tonalitic–trondhjemitic–granodioritic (TTG) crust in the Archean: constraints from phase equilibria modelling. *Precambrian Res.* 287, 73–90.

- Palin, R.M., White, R.W., Green, E.C.R., Powell, R., Diener, J.F.A., Holland, T.J.B., 2016c. High-grade metamorphism and partial melting of basic and intermediate rocks. *J. Metamorph. Geol.* 34, 871–892.
- Pardo, J., Keller, G.R., Holloway, S., 2008. New observations on the extent of Cambrian rifting in Colorado: an update. In: *Geological Society of America*, 40, p. 545.
- Raith, M.M., Rakotondrazafy, R., Sengupta, P., 2008. Petrology of corundum–spinel–sapphirine–anorthite rocks (sakenites) from the type locality in southern Madagascar. *J. Metamorph. Geol.* 26, 647–667.
- Raymond, W.H., Leiggi, P.A., Sheridan, D.M., 1980. Sapphirine in Precambrian rocks associated with stratabound sulfide deposits, Custer County, Colorado. *U.S. Geol. Surv. Bull.* 1513.
- Rivers, T., 2008. Assembly and preservation of lower, mid, and upper orogenic crust in the Grenville Province—Implications for the evolution of large hot long-duration orogens. *Precambrian Res.* 167 (3–4), 237–259.
- Santos, C.A., Moraes, R., Szab'o, G.A.J., 2019. A comparison between phase diagram modelling of metamafic rocks and experimental and independent thermobarometric data. *Lithos* 340, 108–123.
- Sawyer, E.W., 1999. Criteria for the recognition of partial melting. *Phys. Chem. Earth Solid Earth Geod.* 24, 269–279.
- Scrimgeour, I.R., Raith, J.G., 2002. A sapphirine–phlogopite–cordierite paragenesis in a low-*P* amphibolite facies terrane, Arunta Inlier, Australia. *Mineral. Petrol.* 75, 123–130.
- Selverstone, J., Hodgins, M., Aleinikoff, J.N., Fanning, C.M., 2000. Mesoproterozoic reactivation of a Paleoproterozoic transcurrent boundary in the northern Colorado front range: implications for ~1.7- and 1.4-Ga tectonism. *Rocky Mt. Geol.* 35 (2), 139–162.
- Shaw, C.A., Karlstrom, K.E., 1999. The Yavapai-Mazatzal crustal boundary in the southern Rocky Mountains. *Rocky Mt. Geol.* 34, 37–52.
- Shaw, C.A., Karlstrom, K.E., Williams, M.L., Jercinovic, M.J., McCoy, A.M., 2001. Electron-microprobe monazite dating of ca. 1.71–1.63 Ga and ca. 1.45–1.38 Ga deformation in the homestake shear zone, Colorado: origin and early evolution of a persistent intracontinental tectonic zone. *Geology* 29, 739–742.
- Siddoway, C.S., Givort, R.M., Bodle, C.D., Heizler, M.T., 2000. Dynamic versus anorogenic setting for Mesoproterozoic plutonism in the Wet Mountains, Colorado: does the interpretation depend on level of exposure? *Rocky Mt. Geol.* 35, 91–111.
- Sims, P.K., Stein, H.J., 2003. Tectonic evolution of the Proterozoic Colorado province, Southern Rocky Mountains: a summary and appraisal. *Rocky Mt. Geol.* 38, 183–204.
- Taylor, S.R., 1964. Abundance of chemical elements in the continental crust: a new table. *Geochim. Cosmochim. Acta* 28, 1273–1285.
- Taylor, R.B., Stoneman, R., Marsh, S., Dersch, J., 1984. An assessment of the mineral resources potential of the San Isabel National Forest, south-Central Colorado. *U.S. Geol. Surv. Bull.* 1638, 43.
- Warren, R.G., 1983. Metamorphic and tectonic evolution of granulites, Arunta Block, Central Australia. *Nature* 305, 300–303.
- Waters, D.J., 1988. Partial melting and the formation of granulite-facies mineral assemblages in Namaqualand, South Africa. *J. Metamorph. Geol.* 6, 387–404.
- Weller, O.M., St-Onge, M.R., Searle, M.P., Rayner, N., Waters, D.J., Chung, S.L., Palin, R.M., Lee, Y.H., Xu, X.W., 2013. Quantifying Barrovian metamorphism in the Danba structural culmination of eastern Tibet. *J. Metamorph. Geol.* 31, 909–935.
- White, R.W., Powell, R., Holland, T.J.B., Johnson, T.E., Green, E.C.R., 2014. New mineral activity–composition relations for thermodynamic calculations in metapelitic systems. *J. Metamorph. Geol.* 32, 261–286.
- Whitmeyer, S.J., Karlstrom, K.E., 2007. Tectonic model for the Proterozoic growth of North America. *Geosphere* 3, 220–259.
- Wooden, J.L., Miller, D.M., 1990. Chronologic and isotopic framework for early Proterozoic crustal evolution in the eastern Mojave Desert region, SE California. *J. Geophys. Res. Solid Earth* 95, 20133–20146.
- Wooden, J.L., Barth, A.P., Mueller, P.A., 2013. Crustal growth and tectonic evolution of the Mojave crustal province: insights from hafnium isotope systematics in zircons. *Lithosphere* 5, 17–28.
- Zhou, T., Yuan, F., Tan, L., Fan, Y., Yue, S., 2006. Geodynamic significance of the A-type granites in the Sawuer region in west Junggar, Xinjiang: rock geochemistry and SHRIMP zircon age evidence. *Sci. China Ser. D* 49, 113–123.